Assessment of the LPS Ephemeris Accuracy using Inter-Satellite Linking

Master Thesis

C.C. Brunt

Technische Universiteit Delft

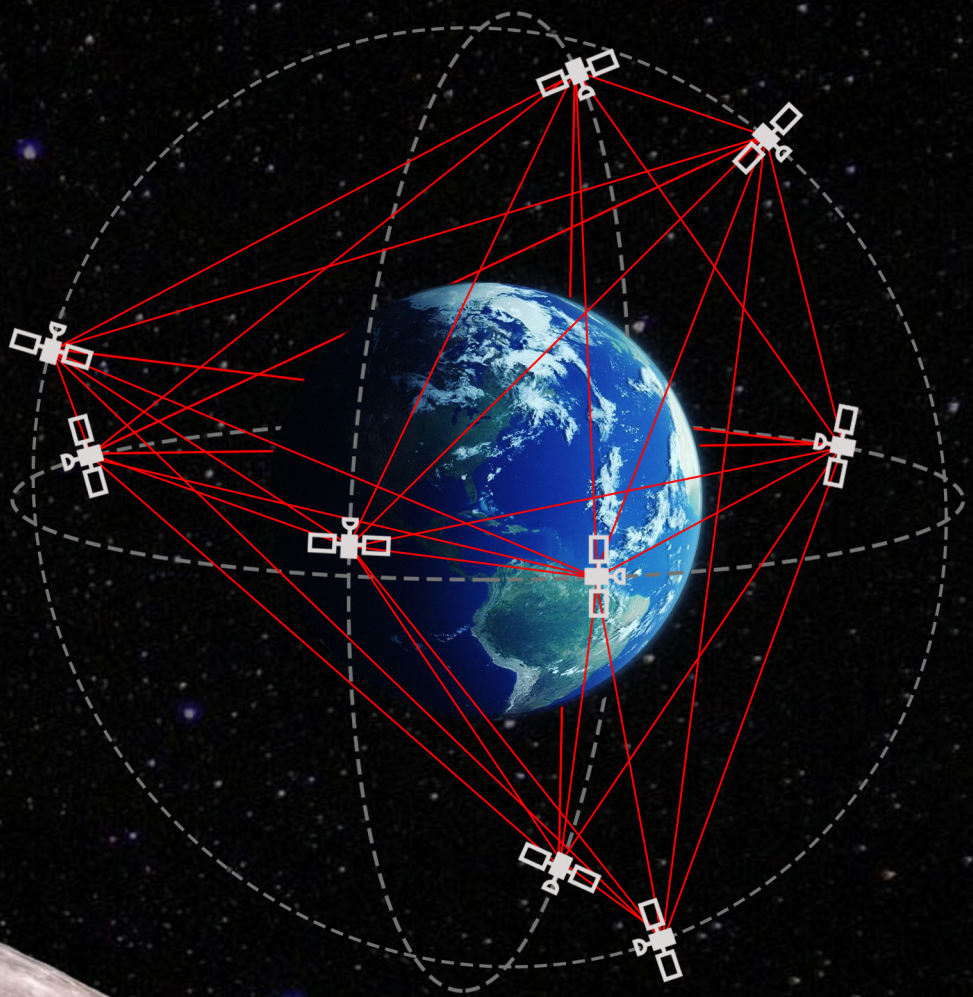

TU Delft

Assessment of the LPS Ephemeris Accuracy using Inter-Satellite Linking

by

Casper Cornelis Brunt

Thesis for the degree of

Master of Science

at The Astrodynamics and Space Missions Section,
Delft University of Technology,
to be defended publicly on Wednesday, June 24th, 2020 at 9:30.

Student number:	4307372	
Thesis committee:	Prof. dr. ir. P.N.A.M. Visser,	TU Delft, daily supervisor
	Dr. ir. E.J.O. Schrama,	TU Delft, committee chair
	Dr. J. Guo,	TU Delft
	Dr. M. Martin-Neira,	ESA ESTEC

TU Delft

Preface

This document is the result of eight months of research on orbit determination and the use of inter-satellite linking supporting a lunar navigation system. It is submitted in partial fulfilment of the requirements for the degree of Master of Science at the faculty of Aerospace Engineering.

This work marks the end of an important period of my life, the years as a student in Delft. It is a period I will always happily and proudly look back at as it formed me to the person who I am now. I have really enjoyed the studying and the student life in Delft. Still, I am thrilled to complete it with the study presented in this document. During the time at the aerospace faculty, I grew an interest in the Moon, and I am pleased to be able to conclude this time with a project contributing to Moon travel.

The quality of this thesis and the form in which it is now, is something that I would not have achieved on my own. Luckily several people offered help during the process. First of all, I want to thank Manuel Martin-Neira, who initiated this research subject. During my research, we only met once. Still, he gave me constructive feedback and ideas for the continuation of the project. Besides, he was quick over the mail and provided me with valuable information and sources. I also want to thank Pieter Visser, my thesis supervisor, with whom I discussed my work every week. With his scientific knowledge, professional attitude and enthusiasm, he guided me through my literature study and the thesis research. The first meeting was over a year ago and since then have always been very helpful, even when the weekly meetings changed to Skype meetings due to COVID-19. Furthermore, I want to acknowledge Marie, who helped me a lot in my battle with Tudat and C++ during the first phase of my research, but also in the last stage by proofreading my work. I would like to thank Mischa as well. He studied the lunar navigation segment of LPS earlier and shared his knowledge about the system with me. In addition, I want to thank my friends from the UFO, who offered some distraction during the many months of research, gave me feedback on my work and helped me with the astonishing looks of this document. Finally, I wish to thank my family and Willemijn, who were always there for mental support, without them it would be difficult to stay motivated all the time.

Casper Cornelis Brunt
Delft, May 2020

Abstract

This thesis work investigates the achievable accuracy of the position determination of a constellation in Polar-Equatorial Circular Medium Earth Orbits (PECMEO) and specifically the improvement of this accuracy by using Inter-Satellite Linking (ISL).

Such a constellation is proposed as an innovative lunar navigation solution based on GNSS technology.

The past decade saw a significant increase in interest in lunar missions after years of other destinations for space travel. Not only traditional space agencies, but also commercial companies have targeted the Moon for current and future missions. The renewed interest is fuelled by the discovery of water on the Moon, the exploitation of lunar resources and plans for the Lunar Gateway. Because of this development, the number of objects around or on their way to the Moon is forecasted to grow significantly. Besides that, the requirements for lunar navigation are expected to increase as well.

This puts much pressure on current lunar navigation solutions, which primarily consist of ground-based tracking systems. This method can only track a limited number of satellites and requires a remarkable amount of infrastructure. Hence, it is not a satisfactory method for the lunar environment considering the current developments. Therefore the need for a reevaluation of lunar navigation rises.

For Earth applications, GNSS is used, providing high accuracy solutions not restricted to a number of satellites. For lunar navigation, however, GNSS is not suitable as the signals are weak, and the coverage is limited at the Moon.

The proposed solution is to deploy a constellation of nine satellites in PECMEO providing a universal lunar navigation system based on GNSS technology: the Lunar Positioning System (LPS). LPS will provide navigation for lunar missions on a more autonomous base and without limitations on the number of receivers.

In order to provide accurate positioning for lunar objects with LPS, the position of the LPS satellites must be known with high accuracy. The ephemeris error, which is caused by the misplacement of the navigation satellites, is one of the most significant error sources in navigation. Especially in lunar navigation executed from the Earth, the ephemeris error can result in substantial inaccuracies as is illustrated in earlier studies.

That is the reason that this thesis work studies the position estimation precision achievable for the satellites in PECMEO. The position estimation of the LPS satellites is based on observations provided by GNSS constellations, but also by precise inter-satellite ranging within the constellation to enhance the position knowledge of the satellites significantly.

The focus of this research is the assessment of the position estimation accuracy of the LPS constellations and, specifically, the enhancement of this accuracy by enabling ISL. The work evaluates the precision of the position determination using Single Point Positioning (SPP) and Kinematic Orbit Determination (KOD) least-squares methods. The satellite positions estimated with these algorithms are compared with the simulated “true” satellite positions to express the performance of the estimation.

In order to correctly perform the estimation for the ISL systems, modified least-squares algorithms have been developed. These algorithms are suitable for observations linked to multiple satellites and the position estimation of those satellites simultaneously.

This thesis extensively assesses the influence of enabling ISL by testing three different ISL systems, each using different measurement techniques. The first system is based on GPS-like observations (GPS ISL), the second system uses a laser ranging instrument (LRI), and the third applies K-band ranging measurements (KBR).

In addition, this work examines the capability of the satellites to synchronise their satellite clocks. This capability is tested for every ISL system. As a result, a total of six different system configurations are considered, which each are compared to the non-ISL solution.

This study identifies two error sources, observation noise and GNSS ephemeris error, in order to

provide relevant insight into the functioning of the different measurements types. The first is a random error source, while the latter is a systematic error source.

This study shows that the average 3-dimensional position error is 7.84 cm for the system that does not make use of ISL if both error sources are included. An average 3-dimensional position error of 2.30 cm for the GPS ISL system and even 1.80 cm for the LRI and KBR ISL system can be achieved by using ISL.

These results show that significant improvements can be realised for the positioning of the LPS satellites when ISL is included in the estimation. While the differences between the various system configurations are small, KBR provides slightly better position estimates. The synchronisation of the satellite clocks does not have a significant impact on the estimation solution in the current set-up.

The achieved accuracy of roughly 1.80 cm is rather high, and with prospected improvements in the solution, flaws in the LPS ephemeris of this level suggest a viable system for lunar navigation.

Contents

Abstract **v**

Nomenclature **xi**

1 Introduction **1**
1.1 Research Questions 2
1.2 Report Outline 3

2 Journal Article **5**

3 Conclusions and Recommendations **67**
3.1 Conclusions 67
3.2 Recommendations 70

A Verification and Validation **71**
A.1 Error-free Simulation Verification 71
A.2 Point Positioning Verification 71
A.3 Analytical Verification 73

B Orbital Parameters **77**

C Software Dependencies **81**

Bibliography **83**

Nomenclature

Abbreviations and Acronyms

DOP	Dilution Of Precision
DSN	Deep Space Network
FoV	Field of View
GDOP	Geometric Dilution of Precision
GLONASS	Global Navigation Satellite System
GNSS	Global Navigation Satellite System
GPS	Global Positioning System
GRACE	Gravity Recovery and Climate Experiment
GRAIL	Gravity Recovery and Interior Laboratory
ISL	Inter-Satellite Linking
KBR	K-Band Ranging
KOD	Kinimatic Orbit Determination
KODISL	KOD for Inter-Satellite Linking
LOP-G	Lunar Orbital Platform-Gateway
LPS	Lunar Positioning System
LRI	Laser Ranging Instrument
LSQ	Least-squares
LTC	Light-time Correction
NASA	National Aeronautics and Space Administration
PECMEO	Polar-Equatorial Circular Medium Earth Orbits
SMA	Semi-Major Axis
SPP	Single Point Positioning
SPPISL	SPP for Inter-Satellite Linking
Tudat	TU Delft Astrodynamics Toolbox
VLBI	Very-Long-Baseline Interferometry

Greek Symbols

δt	Clock Offset	s
ϵ	Observation Error	m
λ	Wavelength	m

μ	Standard Gravitational Parameter	$m^3 s^{-2}$
Ω	Longitude of the Ascending Node	rad
ω	Argument of Periapsis	rad
ϕ	Carrier Phase	rad
ρ	Geometric Range	m
σ	Standard Deviation	$-$
τ	Signal Travel-time	s
θ	True Anomaly	rad

Superscripts

-1	Inverse of Matrix
i	Observation/Satellite Index
s	Transmitting Satellite
T	Transpose of Matrix

Roman Symbols

B	Bias Estimation Parameter Vector	m
e	Line of Sight Vector	$-$
H	Design Matrix	$-$
h	Modelled Observations	m
N	Normal Matrix	m^{-2}
Q	Covariance Matrix	m^2
r	Position Vector	m
W	Weight Matrix	m^{-2}
Y	State Estimation Parameter Vector	ms^{-1}
z	Observation Vector	m
A	Bias Term	m
a	Semi-Major Axis	m
b	Bias Estimation Parameter	m
C	Relative Spacing between Adjacent Planes	$-$
C	Speed of Light in a Vacuum	ms^{-1}
e	Eccentricity	$-$
f	Frequency	Hz
I	Ionospheric Pathdelay	m
i	Inclination	deg
L	Carrier Phase Range	m

M	Number of Bias Parameters	$-$
M	Other Error(s) Term	m
N	Integer Ambiguity	$-$
N	Number of Epochs	$-$
P	Pseudorange	ms
p	Number of Circular Orbits	$-$
R	Radius	m
t	Number of Satellites	$-$
t	Time	s

Subscripts

0	Initial Value
B	Partitioned Bias Design Matrix
BB	Partitioned Bias Matrix
BY	Partitioned Bias-State Matrix
j	Epoch Index
k	Bias Index
KBR	KBR Measurement Error
L	Carrier Phase Measurement Error
LRI	LRI Measurement Error
M	Number of Biases
N	Number of Epochs
P	Pseudo Range Measurement Error
$phase$	Carrier Phase Observation
r	Receiving Satellite
$r*$	Synchronised LPS clock
r_n	Receiving LPS Satellite i
$range$	Pseudo Range Observation
Y	Partitioned State Design Matrix
YB	Partitioned State-Bias Matrix
YY	Partitioned State Matrix

1 Introduction

The interest in the Moon as spaceflight destination decreased significantly after the Space Race between the Soviet Union, and the United States was over its peak, and the US Apollo and the Soviet Luna programs ended in 1972 and 1976, respectively. However, recently, more than 50 years after the first man visited the Moon, a new interest in the Moon has emerged. Fuelled by the discovery of water on the Moon, the idea of establishing a lunar-based refuelling station for more distant missions and the commercialisation of lunar missions, this interest caused the Moon to return on the planning of many space agencies [8] [11]. Existing plans range from scientific orbiters and commercial landers to robotic surface missions and crewed missions [2–4, 9, 12]. There are even plans for placing a crewed space station in the vicinity of the Moon [1]. The enormous increase in the number of missions and their applications is made possible by the technology that has evolved since the 1970s.

Lunar navigation, however, is not keeping up with the technology as it is still primarily done with Earth-based ground tracking. The navigation accuracy that is offered by ground stations is acceptable, but is limited to a number of users and requires remarkable infrastructure. Developing a navigation system for every single mission outside Earths' vicinity would require many large investments and resources. The current navigation solutions for the Moon can not guarantee sufficient accuracy for the rapidly increasing number of lunar missions. For Earth applications, GNSS is used, which allows any new user to make use of its navigation capabilities autonomously. GNSS can not be used for lunar applications to its full extent, but a similar system is desired.

Hence, it becomes clear that, in order to set the next step in space exploration, it is essential to design a universal solution that facilitates more precise navigation and positioning with a high availability on other celestial bodies, beginning with our closest neighbour in the galaxy: the Moon.

The Lunar Positioning System (LPS) is the solution that offers the required improved navigation means for the positioning of objects flying toward, from or on the lunar surface. The concept constellation consists of nine satellites in Polar-Equatorial Circular Medium Earth Orbits (PECMEO).

The lunar navigation is based on the technological principles of GNSS, which means that it transmits navigation signals that can be picked up by any receiver to perform one-way ranging. Hence, any number of future lunar missions is allowed to make use of LPS navigation without degrading the system performance. Moreover, the navigation solution can be used with high autonomy.

To provide accurate lunar positioning, the LPS satellites are required to know their position with high accuracy.

In Earth navigation, one of the most significant error sources is the ephemeris error, which is the displacement of the position of the GNSS satellite leading to an incorrect user position estimation [6]. This means that the correct positioning of the LPS satellites themselves is of great importance in order to facilitate accurate lunar positioning. This is confirmed in an earlier study about LPS, where the ephemeris error of the LPS satellites is shown to be of significant influence on the position estimations of lunar targets [5].

The accuracy of the position estimation of the LPS satellites can, therefore, indicate the limitations or possibilities of the navigation constellation and even point out the feasibility of the LPS concept. Hence, this study will focus on the assessment of the position estimation accuracy of the LPS satellites.

The constellation will make use of the existing GNSS network to determine its satellites position. In addition, the high accuracy of the LPS positioning is specifically expected to be achieved by making use of Inter-Satellite Linking (ISL), allowing the satellites to communicate with each other.

To explore the potential benefits, a method is developed assessing the accuracy of the position estimation of the LPS satellites when different system configurations and environmental models are used. The accuracy assessment is based on existing least-squares estimators, Single Point Positioning (SPP) and Kinematic Orbit Determination (KOD), but the algorithms are rewritten to be suitable for ISL observations. The effects of using different measurements types for the communication between LPS satellites are estimated by considering three different communication systems. The study considers a system using traditional GNSS observation products (GPS ISL), a second system relying on laser ranging instrument measurements (LRI) and third system based on microwave K-band ranging observations (KBR). A variation to the systems is a constellation with the ability to have its satellite clocks in phase. This way, the effect of synchronised clocks is evaluated. To demonstrate the response of the systems to errors, the simulations are also performed with measurement noise errors and GNSS ephemeris errors included in the model. The two different types of errors have been selected to show the behaviour of the system under the influence of systematic and random errors.

The presented study aims to determine with which precision the position of the LPS satellites can be estimated and in particular to demonstrate the impact that inter-satellite linking has on this. The LPS positioning assessment is an essential contribution to the innovative concept of Moon navigation as it uncovers the limitations and expectations of the system. The concept is expected to have improvements in accuracy and availability in comparison with traditional navigation methods. This way, a first step in planetary exploration is presented in the form of an initial design for a new Moon navigation concept. In addition, the use of ISL is studied to a great extent, showing what contribution it has to orbit determination and what form of ISL is most suitable for this.

1.1. Research Questions

The introduction shows that this thesis focuses on determining the ephemeris accuracy of LPS satellites in a PECMEO constellation and the improvement of this accuracy that can be achieved by using different forms of ISL when least-squares estimation methods are applied. The accuracy of these different types are assessed by comparing the estimated satellite positions with the “true” simulated positions. To this extent, the following research questions and sub-questions have been formulated:

1. ***What modifications of existing least-squares algorithms are required to make them suitable for navigation using ISL?***
   (a) *What are the differences between standard observations and ISL observations?*
   (b) *What modifications are required in the SPP algorithms to make them suitable for ISL observations?*
   (c) *What modifications are required in the KOD algorithms to make them suitable for ISL observations?*
   (d) *What modifications are required in the LSQ algorithms to make them suitable for systems with synchronised clocks?*
2. ***What improvement in the accuracy of the position estimation of the LPS satellites can be achieved using Inter-Satellite Linking?***
   (a) *What position accuracy can be achieved for the LPS satellites using an SPP LSQ estimator without ISL observations?*
   (b) *What position accuracy can be achieved for the LPS satellites using a KOD LSQ estimator without ISL observations?*
   (c) *What position accuracy can be achieved for the LPS satellites using a KOD LSQ estimator with ISL observations?*
   (d) *What is the impact on the position accuracy of using different measurement system configurations?*

(e) *What is the impact on the position accuracy of the synchronisation of the LPS satellite clocks?*

(f) *What is the impact on the position accuracy of including random and systematic error sources to the model?*

By answering these research questions, this work can be considered a valuable and substantial contribution to the LPS mission concept and orbit determination applications that make uses of inter-satellite links. The insight in the technical performance of LPS positioning gained through answering the questions can be compared to the requirements and performance of alternatives to obtain an indication of the feasibility of the system. The algorithms developed for position determination that allows for inter-satellite observations, a capability that is shown to be very promising, can be used in future research in this subject.

1.2. Report Outline

The main part of this thesis report is written in the format of a draft journal paper that may be submitted to "Advances in Space Research", published by Elsevier. The paper is written according to the guidelines issued by Elsevier[1]. The paper, titled "*Assessment of the LPS Ephemeris Accuracy using Inter-Satellite Linking*", is presented in chapter 2. The paper begins with an abstract and an introduction; followed by a detailed description of inter-satellite linking. After that, the methodology of this research is presented, explaining the assessment cases and the modified estimation algorithms. Then the simulation environment is clarified, followed by the results and a discussion about the results. The paper ends with the conclusions of the research.

After the paper, chapter 3 aims to answer the research questions posed before. The chapter gives the conclusions of the research and also presents recommendations for future work. Next, the verification and validation of the used models is given in Appendix A. In the chapter, three different verification methods are discussed. Finally, in the last two appendices, the initial Kepler elements of the satellites simulated in the thesis work are displayed and the software used is mentioned. These aspects are showed in Appendix B and Appendix C, respectively.

[1] https://www.elsevier.com/journals/advances-in-space-research/0273-1177/guide-for-authors

2

Journal Article

This chapter presents the stand-alone journal article. This draft paper presents the core of the research for this thesis.

Assessment of the LPS Ephemeris Accuracy using Inter-Satellite Linking

C.C. Brunt[a]

[a]*Delft University of Technology, Kluyverweg 1, 2629HS Delft, The Netherlands*

Abstract

With the increasing interest in lunar missions, the number of objects around the Moon as well as positioning accuracy demands around the Moon increase. Therefore the need for a reevaluation of lunar navigation rises as current solutions, like ground tracking, can not keep up with both aspects. For Earth applications, GNSS is used, providing high accuracy solutions not restricted to a number of satellites. For lunar navigation, however, GNSS is not suitable as the signals are weak, and the coverage is limited at the Moon. The proposed strategy is to deploy a constellation in Polar or Equatorial Medium Earth Orbits (PECMEO) based on GNSS technology, which can be utilised as universal lunar navigation system: the Lunar Positioning System (LPS). The system is expected to provide navigation for lunar missions on a more autonomous base and without limitations on the number of receivers as is the case for current lunar navigation solutions. However, for the nine LPS navigation satellites to provide accurate positioning for lunar objects, it is crucial that the positions of the satellites themselves are estimated with high accuracy. This is because the ephemeris error of navigation satellites is a dominant factor in the eventual position error of lunar objects. This paper investigates the achievable orbit determination solution for the satellites in PECMEO. The position estimation of the LPS satellites is based on observations provided by GNSS constellations, but also by precise inter-satellite ranging within the constellation to enhance the position knowledge of the satellites significantly. This research focuses on the feasible position estimation of the LPS satellites and, specifically, what improvements can be achieved by including ISL in the estimation. An expression of the perfor-

Email address: C.C.Brunt@student.tudelft.nl (C.C. Brunt)

mance of the system is obtained by estimating the satellite positions using point position and kinematic orbit determination least-squares methods. In order to correctly perform the estimation for the ISL systems, modified least-squares algorithms have been developed suitable for observations linked to multiple satellites and the position estimation of those satellites simultaneously. To extensively assess the ISL influence, three systems are tested in the study, each using different measurement techniques. One based on GPS-like observations (GPS ISL), another using laser ranging (LRI) and a third applying K-band ranging measurements (KBR). Furthermore, the capability of the constellation to have all its satellite clocks in phase is investigated, leading to a total of six different system configurations which are compared to the non-ISL solution. In the study two error sources are identified, observation noise and GNSS ephemeris error, which give valuable insight into the behaviour of the different measurements types as the former is a random error source, while the latter is a systematic error source. In the case that both error sources are included, the average 3-dimensional position error is 7.84 cm if no ISL is used. When ISL is added to the estimation, the average 3-dimensional position error reduces to 2.30 cm for the GPS-like ISL system and even to 1.80 cm for the LRI and KBR ISL systems. Therefore, it is shown that significant improvements can be achieved for the positioning of the LPS satellites by using ISL. While the differences between the various system configurations are small, KBR provides slightly better position estimates. Phasing of the satellite clocks does not have a significant impact on the estimation solution in the current set-up. The achieved accuracy of roughly 1.80 cm is rather high, and with prospected improvements in the solution, flaws in the LPS ephemeris of this level suggest a viable system for lunar navigation.

Keywords: lunar navigation, orbit determination, least-squares, inter-satellite linking, kinematic orbit determination

1. Introduction

More than 50 years after the first man visited the Moon [1], a new interest in the Moon has emerged. The number of planned missions to the Moon is rising as many space agencies prepare for a new visit. NASA has put great emphasis on the Moon in its road map with orbiters, commercial landers and robotic surface missions, but also crewed missions [2]. There are even

plans for placing a crewed space station in the vicinity of the Moon [3] that supports for lunar exploration opportunities, but also functions as a gateway to other destinations in the Solar System. Besides that, space agencies from Japan, Korea and India are operating or planning lunar missions, and also China has an extensive lunar exploration program [4, 5, 6, 7]. The discovery of water ice on the Moon and the idea of establishing a refuelling station for more distant missions using this water is one of the reasons for this renewed interest in the Moon [8, 9]. The commercialisation of the exploitation of lunar resources [10] is another aspect that fuels this interest.

For Earth applications, GNSS offers very accurate navigation solutions for an unlimited number of users. However, using GNSS for lunar navigation shows to be difficult for three reasons: its low transmission power, Earth nadir pointing, and the significant signal travel distance. Therefore, the positioning of objects on and around the Moon is currently primarily performed with Earth surface-based tracking systems. The systems offer navigation, but it is limited in its accuracy and number of users compared with GNSS. This is because the several ground stations are required to track a specific mission, so the availability of this solution is low. Meanwhile, lunar missions evolve, the operations get more complex and more accurate positioning is required. Moreover, the number of missions increases vastly. There are missions mapping the lunar surface [11, 12, 13], sample-return missions, requiring rendezvous, docking and landing [14, 15, 16, 17], and also missions operating a robotic rover or lander [18, 4, 19]. All these types of mission need significant position accuracy, for safe execution of their operations and to increase their scientific return. The current navigation solutions for the Moon can not guarantee sufficient accuracy for the rapidly increasing number of lunar missions. Designing and developing a navigation system for every single mission outside Earths' vicinity would require many large investments and resources. Hence, it becomes clear that, in order to set the next step in space exploration, it is essential to design a universal solution that facilitates more precise navigation and positioning with a high availability on other celestial bodies, beginning with our closest neighbour in the galaxy: the Moon.

The Lunar Positioning System (LPS) is the solution that offers the means for the required improved positioning. The concept constellation consists of nine satellites in medium-Earth orbit with three orthogonal orbital planes, one equatorial and two polar planes. From these Polar-Equatorial Circular Medium Earth Orbits (PECMEO), the positioning of objects flying toward, from or on the lunar surface is performed [20].

The lunar navigation is based on the technological principles of GNSS, which means that it transmits navigation signals that can be picked up by any receiver to perform one-way ranging. Hence, the multiple access feature is available, allowing any number of future lunar mission to make use of LPS navigation without degrading the system performance. Moreover, GNSS revolves around the capability of receivers to perform an onboard navigation solution computation without depending on external interaction. This leads to a much higher level of autonomy of the spacecraft by using the one-way ranging instead of other means of ranging methods. A higher autonomy naturally means less operators required for the mission, reducing its operation costs. It also means that, as the system is dependent on less (external) factors, the amount of points of failure is reduced. An increasingly recurring requirement for spacecraft is the ability to return to Earth without contact with Earth [21]. By equipping the spacecraft with an LPS receiver, this requirement can be met using the LPS navigation. This is a more reliable and safer method than using an optical sextant as was done in the past for the Apollo missions, but also is recently tested as a viable emergency navigation method for missions such as Orion and LOP-G [22].

In order to provide accurate lunar positioning, the LPS satellites are required to know their position with high accuracy. The constellation will make use of the existing GNSS network to do this and hence will be placed in an orbit below the conventional GNSS. Besides that, the system will make use of Inter-Satellite Links to further improve its own position solution [20]. The complete navigation system consists of two steps. First, determining the positions of the LPS satellites and second, the positioning of the lunar targets from the LPS satellites. This study focuses on the first step in the LPS, namely the position determination of the LPS satellites themselves.

In Earth navigation, one of the most significant error sources is the ephemeris error, which is the displacement of the position of the GNSS satellite leading to an incorrect user position estimation [23]. This means that the correct positioning of the LPS satellites themselves is of great importance in order to facilitate accurate lunar positioning. This is confirmed in an earlier study about LPS, where the ephemeris error of the LPS satellites is shown to be of significant influence on the position estimations of lunar targets. While the study still deems the navigation accuracy acceptable for Apollo-like lunar spacecraft, it also shows that an error in the LPS positions of only 1.78 cm can already cause errors in lunar positioning of 27.0 m when kinematic orbit determination is used [24]. This outcome stresses the importance of correct

ephemerides knowledge and thus of the position determination of the LPS satellites for the performance of lunar navigation. The accuracy of the position estimation of the LPS satellite can, therefore, indicate the limitations or possibilities of the navigation constellation and even point out the feasibility of the LPS concept.

The high accuracy of the LPS positioning is specifically expected to be achieved by making use of Inter-Satellite Linking (ISL), allowing the satellites to communicate with each other. Substantial improvements in the accuracy of the LPS position determination are expected because of the relative positioning of the satellites, an increase in observations and the geometry improvements. Other gains are expected through the choice of measurements used for the satellite-to-satellite observations. Inter-satellite linking has been done before, like for GRACE and GRAIL [25, 11], but not to the extent of coupling nine satellites on a continuous base.

The aim of the current study is to determine with which precision the position of the LPS satellites can be determined and in particular to demonstrate the impact that inter-satellite linking has on this. The LPS positioning assessment is an essential contribution to the innovative concept of Moon navigation as it uncovers the limitations and expectations of the system. The concept is expected to have improvements in accuracy and availability in comparison with traditional navigation methods. This way, a first step in planetary exploration is presented in the form of an initial design for a new Moon navigation concept. Furthermore, the use of ISL is studied to great extent, showing what contribution it has to orbit determination and what form of ISL is most suitable for this.

To explore the potential benefits, a method is developed assessing the accuracy of the position estimation of the LPS satellites when different system configurations and environmental models are used. An approach is written to incorporate the additional ISL measurements in two existing least-squares estimation schemes: Single Point Positioning (SPP) and Kinematic Orbit Determination (KOD) [26, 27]. The implications of adding the ability to estimate multiple positions simultaneously and including intercorrelated measurements to the schemes are studied and presented. Moreover, the type of system that is used for ISL is also addressed in this study, assessing the effects of having different types of measurements used for the communication between LPS satellites. The performances of systems using traditional GNSS observation products, laser ranging measurements and K-band microwave observations are determined and compared. In addition, the ability of the

LPS satellites to have their clocks in phase is evaluated. When the satellites have the same clock, only one clock offset parameter has to be estimated instead of one for every LPS satellite, which can be assumed to improve the estimation results. To get a more complete view on the technical performance of the different systems, the simulations are also performed while errors are included to demonstrate the response of the systems. Two different types of errors have been selected to show the behaviour of the system under the influence of systematic and random errors. These errors are GNSS ephemeris errors and measurement noise errors and their effect on the position accuracy is also treated in this study.

The methodology to estimate positions while using inter-satellite links of a constellation developed in this paper is derived for a specific science case. Still, it can be applied to other constellations that stabilise their position solution using inter-satellite linking.

This paper is organised as follows. In Section 2, a detailed description of inter-satellite linking, its advantages and its implications are presented. The assessment cases for this study and the methodology used to assess the position determination performance of the various systems are then described in Section 3, followed by the environment and system set-up and the simulation of the orbits and observations in Section 4. The results of the orbit determination of the different assessment cases are presented in Section 5. After that, the results and their implications for the lunar navigation concept are discussed in Section 6. Finally, in Section 7, the conclusions and some final remarks are stated.

All the numerical simulations presented in this paper have been conducted with the Tudat toolkit developed by the Astrodynamics & Space Missions department of Delft University of Technology (see Appendix C in [28]).

2. Inter-Satellite Linking

This section gives a detailed elaboration on Inter-Satellite Linking. ISL is a form of space-to-space interferometry, where two or more satellites are communicating with each other to exchange data for various purposes.

It is a technique that is currently being studied increasingly. Concepts exist that use ISL to facilitate space-to-space very-long-baseline interferometry (VLBI) providing an innovative imaging system [29, 30]. Other authors describe using ISL for two satellites to facilitate autonomous orbit determination, i.e. without the help of GNSS or ground-based tracking systems

[31, 32]. The fruitful GRACE and GRAIL missions depended on ISL to improve their scientific return [25, 11] and applying ISL to allow for distributed satellite systems is considered as well [33, 34].

The main advantage of applying space-to-space interferometry in this study, however, is the significant improvement in the precision of the position estimation. Subsection 2.1 explains the gains of ISL for orbit determination accuracy specifically. To better understand the benefits of ISL for this specific mission, the subsection elaborates on the PECMEO constellation as well.

To conclude this section, the implications of incorporating ISL in the estimation are described in Subsection 2.2.

2.1. Position Accuracy Advantages

The accuracy of the position solution can be improved by the inclusion of ISL in multiple ways which are discussed in the subsequent sections.

2.1.1. Additional Observations

ISL enables communication links between the satellites in the LPS constellations and this way the satellites can receive observations from each other to enhance the estimation solution. The increase in the number of observation is one of the reasons for the improvement in the orbit determination accuracy, as suggested by [35]. Figure 1a shows how many satellites are available on average per LPS satellite during one day, in this case four GNSS constellations are considered: Galileo, GLONASS, BeiDou and GPS. The figure shows that when ISL observations are also used the number of satellites available on average increases by more than seven, which means seven more observations per epoch.

2.1.2. Orbital Geometry

Another reason for the improvement in position accuracy is the improved geometry of the system. This has to do with the Dilution of Precision (DOP), which is a way to express the geometric distribution of a navigation system. In [36] the DOP is explained with visual aid and stresses the importance of the geometric distribution of navigation satellites relative to the user. In this study, there are multiple users, namely the nine LPS satellites. The GNSS satellites are the navigation satellites in this case. The DOP of a constellation relates to the formal accuracy a navigation solution provides. The higher the DOP value, the bigger the error in the formal estimation solution. For this study, a tool is developed determining the DOP value

for different configurations of the LPS constellation following the theory in [36]. In general, the formal error can be determined by taking the square of the correct diagonal values in the covariance matrix, which is the inverse of the normal matrix in the navigation solution. For the illustration of the ISL benefits, at this stage, only the normal matrix of a simple navigation solution is considered as opposed to also using the normal matrix of the kinematic navigation solution.

The orbital design of the LPS affects the benefits gained by including ISL. Like mentioned before, the constellation is placed in three orthogonal orbital planes, two polar and one equatorial, with three satellites in each plane. The satellites are equally distributed over the orbital planes at a radius of 14,000 km, this way all LPS satellites are visible for each other at almost any moment [20]. Only when the Earth is blocking the view between two satellites, the inter-satellite link is lost temporarily. Because of this dispersion, the ISL observations give the constellation an outstanding geometric distribution. In combination with the standard links with the GNSS satellites, which are in much higher orbits, an excellent geometric distribution is obtained. Section 4 further elaborates upon the orbital arrangement and the observations.

Figure 1b shows the improvement in the Geometric DOP (GDOP) values caused by using ISL compared to the non-ISL configuration. The GDOP is not only two times smaller on average, but it is also much more stable over time. This means that the position error is expected to be significantly smaller when ISL is enabled. Besides that, the more stable values imply that less sudden drops in precision occur in the estimation process, leading to less unpredictable situations. This suggests that, considering the geometry of the problem, adding the possibility of inter-satellite linking can result in vast improvements in the positioning of the satellites, including enhanced robustness.

Another advantage of the space-to-space interferometric system at the proposed PECMEO altitude is the absence of any atmospheric effect on the ISL [20]. This includes most of the effects of the ionosphere, which is the most significant source of errors in many GPS applications [30]. This means that the measurements shared between the satellites are less affected because of the selected height regime.

2.1.3. Type of Measurements

In addition, the ISL can consist of other observation types than the traditional GNSS satellites observations and these different types of measure-

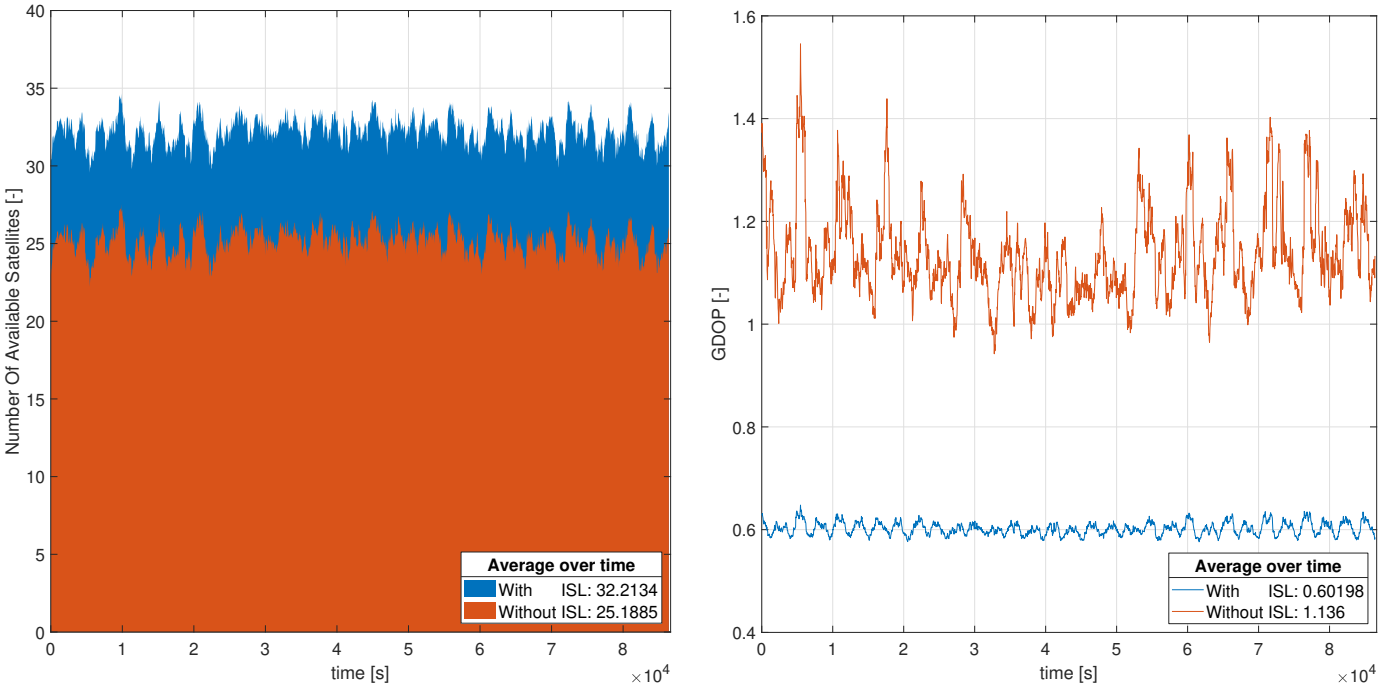

(a) Number of available satellites over time

(b) GDOP value over time

Figure 1: The number of available satellites (Galileo, GLONASS, BeiDou, GPS or LPS) and GDOP value over time, averaged over the LPS satellites

ments can significantly improve the estimation solution. By using systems that provide much more accurate measurements of the inter-satellite distance, positioning can be performed very precisely, hence improve the overall navigation solution. The GRACE mission did this by deploying two satellites that made use of ISL K-band ranging (KBR) to achieve very small errors in relative position determination [25], and the GRAIL mission did the same around the Moon [11]. The successor of the former, the GRACE Follow-On mission, even uses a laser ranging interferometer (LRI) instrument to further improve the ranging measurements between two satellites [37].

This means that the ISL system can be a system comparable to the communication system of GNSS links. In this case, the links between the LPS satellites consist of pseudorange code measurements and carrier phase measurements with the same quality as for GNSS observables. The pseudorange code measurements can be used directly, but for the carrier phase measurements an ambiguity has to be determined to use them. This means an extra

parameter to estimate, but in general a more precise measurement. This way, the ISL can be treated as an additional GNSS constellation in the simulation.

A second way to perform the ISL is to use optical laser ranging measurements, like on the GRACE Follow-On. An LRI instrument can be used to obtain observations that are highly accurate and unambiguous. This system configuration is treated slightly different in the simulation, because the additional observations are pseudorange-like measurements, and there are no phase-like measurements that require additional estimation parameters.

The third system configuration that is considered is comparable to the GRACE satellite-to-satellite interferometry, using K-band ranging (KBR) measurements. This observable type has a much higher accuracy than the traditional GNSS-like observations, but does require for an ambiguity to be estimated. Therefore it can be treated like the phase measurement in the simulation process, while there is no code-type measurement. These three measurement types are distinguished and used in this study to examine the influence of the different measurement accuracies and to show the improvements that can be achieved by employing ISL in combination with non-traditional, more accurate observations.

Section 4 gives a more thorough explanation about the observations and differences between the selected types.

2.1.4. Clocks in Phase

Another asset of allowing the communication between the satellites is the ability to have the satellite clocks in phase. In other words, the clocks of the separate satellites are equivalent, and the clock offset per epoch is identical for the entire system. This means that during the estimation instead of nine clocks, only one clock has to be estimated per epoch. Less parameters to estimate in general implies a more accurate overall estimation solution. Subsection 3.3 elaborates on this subject. This work also considers a version of all three systems mentioned above with the clocks in phase. This way, there are six different ISL system configurations that are considered in this study beside the benchmark non-ISL configuration.

2.2. Implications

Besides the anticipated outcomes described, there are also negative consequences of the utilisation of ISL. The first thing to realise is that in order to use an observation, the position of the corresponding transmitter should be known. The GNSS satellites broadcast their position to the receivers,

but for an ISL observation, the transmitters' position is not known as it is being estimated as well. Hence, in contrast to estimating the positions of the LPS satellites separately one-by-one, a solution has to be found for the entire constellation simultaneously, and the positions of all nine satellites have to be estimated at once. Hence, the mathematics involved with the estimation process increase in complexity and dimension. Instead of determining the position and clock offset of one satellite, which are four parameters, the position and clock offset of all satellites have to be determined, resulting in 36 parameters. Besides that, interference between the satellites has to be incorporated in the estimation algorithms leading to the need of cautiously handling all the observations and their arrangement in the matrices. The effects of ISL on the mathematics of the navigation problem are discussed in more detail in the following section.

3. Methodology

This section describes the overall methodology used to achieve the research goal. First, the different test cases are presented, followed by the general method to assess the LPS positioning performance. Finally, the navigation algorithms and mathematical strategies are explained in more detail.

3.1. Assessment Cases

This study recognises seven distinct system configurations in four separate noise cases, which are presented in Table 1. The first system is used as a benchmark and does not use ISL for its position determination, but only the four GNSS constellations: Galileo, GLONASS, BeiDou and GPS. The other system configurations consist of three different measurement systems for space-to-space interferometry, each with an additional configuration in which the satellite clocks are synchronised. The first ISL system uses observations similar to GPS observations and is called GPS ISL. The second system, LRI ISL, is based on laser ranging. KBR ISL is the third configuration and applies K-band ranging. Together, the configurations provide a good overview of the effect of ISL with different types of measurements.

The study limits itself to two distinct error sources: measurement noise and GNSS ephemeris errors. These errors are chosen because of there distinct nature; the former is a random error function, while the latter is a systematic error. The response of the navigation system on different incorrect inputs

can be assessed this way. Besides that, the ephemeris error is one of the most significant error sources in most GPS applications.

Section 4 discusses the exact simulation set-up of the system configurations and error cases in more detail.

	No Error	Noise Error	Ephemeris Error	Both Error Sources
GNSS Only				
GPS ISL				
GPS ISL (1 clock)				
LRI ISL				
LRI ISL (1 clock)				
KBR ISL				
KBR ISL (1 clock)				

Table 1: The 28 different simulation cases used in the study

3.2. General Methodology

The assessment of the LPS position determination performance and specifically the influence of the ISL system variations on this is performed by a tool developed to numerically determine the accuracy of the position estimation of the satellites. The accuracy of the position estimation is determined by looking at the difference between the estimated satellite positions and the "true" satellite positions.

The latter are the simulated LPS positions, which the tool generates in the first step. In this step, the positions of the LPS satellites and the GNSS satellites are generated based on the dynamical model, simulation period and orbital elements. The ephemerides of the satellites are also produced in this step. These are used in the navigation algorithms, but also in the observation simulation step. In this second step, beside the ephemerides, the Earth shape model and observation types and their noise errors are required to simulate the observations done by the LPS satellites. The functioning of the first two steps and their inputs are discussed in more detail in Section 4.

The third step consists of the navigation calculations; this is the most extensive segment of the tool and is thoroughly explained in subsequent parts of this section. From this block the estimation results of the different test cases are retrieved. In the last segment of the tool, these estimation results are compared with the true satellite positions to determine the accuracies of the various systems for selected error sources. The results are also compared with each other to get a good overview of the performance of the systems.

Figure 2 shows the flow of activities of the navigation system assessment described. The blocks in the figure correlate to the steps mentioned above. Left in the figure the generation and handling of the correct positions is seen and on the right side of the figure the flow of information for the position estimation is shown. All is synthesised in the lower left of the figure to arrive at the estimation accuracy.

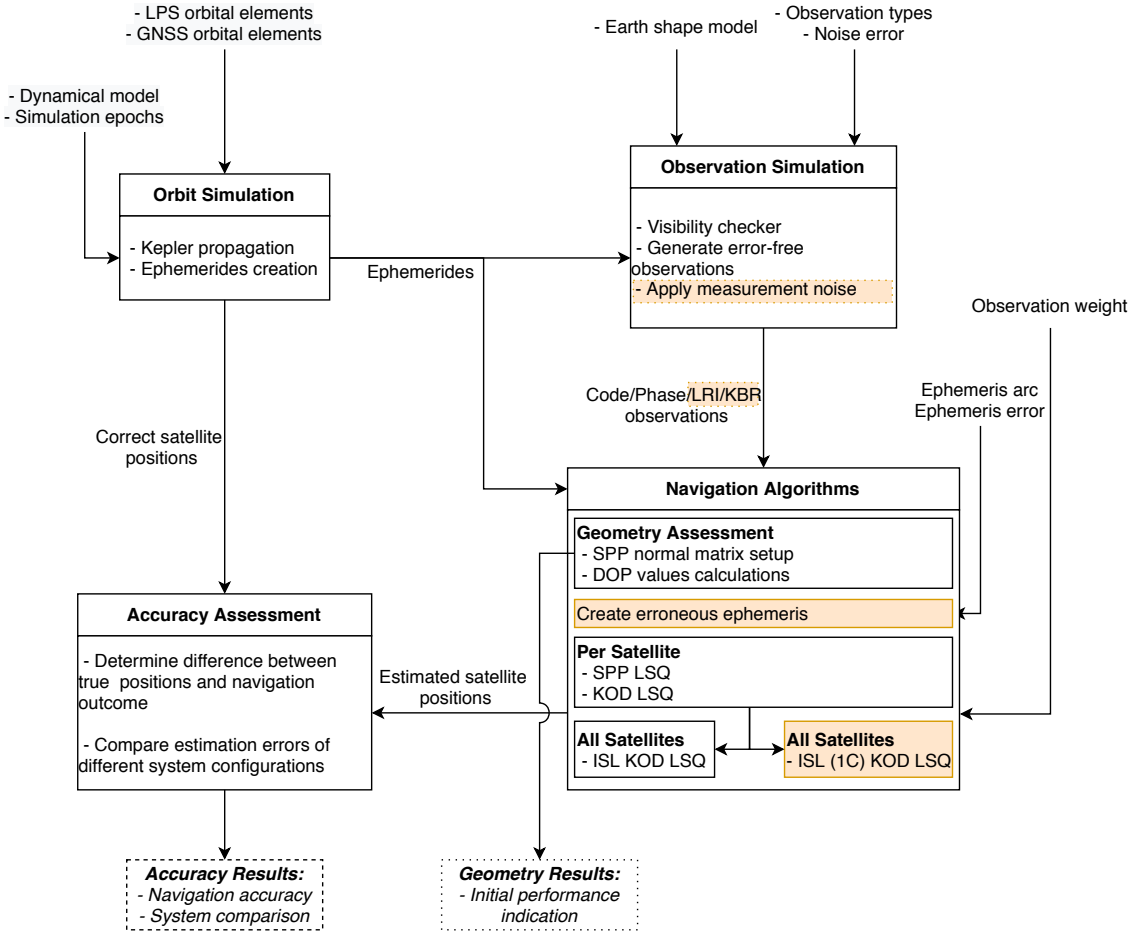

Figure 2: Flowchart showing the steps in the assessment of the LPS positioning performance

3.3. Estimation Techniques

Navigation algorithms are used to obtain estimated spacecraft positions from the observations. This study considers two different algorithms: the Single Point Positioning (SPP) and Kinematic Orbit Determination (KOD) linearised least-squares (LSQ) methods. Both these existing methods are extended during this study to a form that is also suitable to be used with Inter-Satellite Linking. These estimators both make use of an iterative least-squares process to determine the parameters that most accurately fit the observations. The iterative process is necessary since the observation equations are non-linear, as shown in the following subsection. First, a general iterative least-squares process is outlined. After that, two sections shortly describe the existing SPP and KOD algorithms, respectively, to clearly illustrate the adjustments required to create the Single Point Positioning for Inter-Satellite Linking (SPPISL) and Kinematic Orbit Determination for Inter-Satellite Linking (KODISL) algorithms. This description is followed by an explanation about the different forms of the algorithms required for the different simulation cases considered in this study. Table 2, which is found at the end of Subsection 3.3.6, gives an overview of the dimensions of the parameter estimation problem solved by the developed tool.

3.3.1. Modelled Observations

This work considers four different measurements: pseudorange code measurements (GNSS), laser range measurements (LRI, simulated as 1-way measurements), carrier phase measurements (GNSS) and K-band range measurements (KBR). The first two measurements are unambiguous and can be used directly, while for the carrier phase and K-band measurements, an ambiguity has to be determined as well. Section 4 discusses the behaviour and appearance of the measurements in more detail. For now, the difference in modelling of the two different types is important to understand. The first type, from now on referred to as range observation, can be modelled according to Equation 1, while the other type, referred to as phase observation, is modelled according to Equation 2.

$$h^s_{range,r}(t) = \rho^s_r(t) + c\delta t_r(t) - c\delta t^s(t) \tag{1}$$

$$h^s_{phase,r}(t) = \rho^s_r(t) + c\delta t_r(t) - c\delta t^s(t) - b^s_r \tag{2}$$

$h^s_{range,r}(t)$ is the modelled range observation and $h^s_{phase,r}(t)$ is the modelled phase observation. In both equations the first term is the geometric range, $\rho^s_r(t) = \|\mathbf{r}_r(t) - \mathbf{r}^s(t)\|$. $c\delta t_r$ and $c\delta t^s$ represent the clock offsets of the receiver and the transmitter, respectively. In general, when the transmitter is a GNSS satellite, it is assumed that the transmitter clock offset is broadcasted and therefore not estimated. The difference between the two models is the ambiguity, b^s_r, in the modelled phase observation that also has to be estimated. It should be noted that the light-time effect is ignored here, as is explained in Section 4. In the observations equations, a dependency on the receivers' position is seen; the equation for computing the norm of the the vector difference is non-linear, therefore, the equations are non-linear, and an iterative least-squares has to be used to solve the problem.

3.3.2. Iterative Least-Squares

To solve non-linear estimation problems, such as satellite positioning applications, the problem is linearised around an initial value, and an iterative LSQ is used to update that value. This way, the estimation parameters, $\mathbf{y}$, in the navigation measurement model, $\mathbf{h}(\mathbf{y})$, linearised around initial value, $\mathbf{y}_0$, are updated by $\mathbf{y} = \mathbf{y}_0 + \Delta\mathbf{y}$, where Equation 3 gives the LSQ update.

$$\Delta\mathbf{y} = \left(\mathbf{H}^T\mathbf{W}\mathbf{H}\right)^{-1}\mathbf{H}^T\mathbf{W}\left(\mathbf{z} - \mathbf{h}(\mathbf{y}_0)\right) \tag{3}$$

In this equation vector $\mathbf{z}$ consists of the actual navigation measurements. $\mathbf{W}$ is the weight matrix, ideally filled by the inverted covariance matrix of the observations. In this study, however, the inverse of the estimated variances is used and the measurement errors are thus assumed uncorrelated. This provides sufficient realistic weight values for this stage of the study and does not require extensive additional analysis to determine the variable weights. Besides that, in reality, when the navigation solution is to be provided in real-time, the actual observation covariances are not available during navigation.

Then, the design matrix, $\mathbf{H}$, is formed by the partial derivatives of the modelled measurements with respect to the estimation parameters: $\mathbf{H} = \frac{\partial \mathbf{h}(\mathbf{y}_0)}{\partial \mathbf{y}_0}$. Therefore, it is required to parameterise the modelled observations by the parameters to be estimated in order to obtain the partial derivatives. This way $\mathbf{H}$ always has the dimensions of m, the number of observations, by n, the number of parameters to be estimated and $\mathbf{W}$ is a $m \times m$ matrix. The part in Equation 3 that is inverted is also called the normal equations, given by: $\mathbf{N} = \mathbf{H}^T\mathbf{W}\mathbf{H}$.

3.3.3. Single Point Positioning

In SPP the iterative LSQ algorithm is applied using the code observations of a single epoch to determine the position and the receiver clock correction estimates for that particular epoch. This way, only the pseudorange measurements, modelled by Equation 1, are used, and the processing happens epoch-by-epoch. Therefore, the information between different epochs is not correlated, and for every satellite at any observation epoch t, the observation equation is parameterised with the receiver position and the receiver clock offset. Hence, the parameter vector is $\mathbf{y} = (x_r, y_r, z_r, c\delta t_r) = (\mathbf{r}_r^T, c\delta t_r)$.

This way the design matrix gets the form $\mathbf{H}^i = \left(\frac{\partial \mathbf{h}_r^i}{\partial x_r}, \frac{\partial \mathbf{h}_r^i}{\partial y_r}, \frac{\partial \mathbf{h}_r^i}{\partial z_r}, \frac{\partial \mathbf{h}_r^i}{\partial c\delta t_r}\right) = (\mathbf{e}_r^{iT}, 1)$, where superscript i denotes the observation associated with navigation satellite i and its corresponding row in the matrix. $\mathbf{e}$ is the unit vector pointing from the receiver to the transmitter and is given by the partial derivatives of the geometric range, shown in Equation 4. This means that the design matrix has dimensions of the number of observations n-by-four in this case. It should be noted that the position vector of the transmitter r^s is retrieved from the simulated ephemerides of the GNSS satellites.

$$\mathbf{e}_r^s(t) = \frac{\mathbf{r}_r(t) - \mathbf{r}^s(t)}{|\mathbf{r}_r(t) - \mathbf{r}^s(t)|} \tag{4}$$

The code measurements are assumed to be uncorrelated and to have equal noise standard deviations and variances as the same type of the measurements are used. Hence, the weight of the measurements is equal. Therefore the weight matrix is an identity matrix with dimension m. The normal matrix $\mathbf{N}$ for this algorithm is a 4×4 matrix, for the number of parameters to be estimated.

For every single LPS satellite and every epoch, the calculation in Equation 3 is performed, and iterated until the biggest value in the parameter update is smaller than 10^{-5} m.

SPP is the most simple and straightforward method to perform position estimation. It does not provide very accurate solutions for the positioning because only code measurements are used, which generally have meter precision, as is explained in Section 4. Therefore SPP is used as an a priori estimation for the subsequent least-squares estimators in this work.

3.3.4. Kinematic Orbit Determination

The KOD method processes the navigation observations in batch, meaning that it processes the information of a series of epochs at once. Now the epochs are correlated, and the carrier phase measurements can also be used, which tend to have much lower noise and therefore lead to more precise position estimation. The carrier phase observations are ambiguous, thus, a bias estimation has to be included to approximate the integer ambiguity term that appears in the phase measurements with a float value.

This way, every epoch t_j the parameterisation has to be done with $\mathbf{y}_j = (x_{r,j}, y_{r,j}, z_{r,j}, c\delta t_{r,j}) = (\mathbf{r}_{r,j}^T, c\delta t_{r,j})$, but also with the bias parameter b_k that the phase observation contains.

The parameters to be estimated are described by [38] as $\left(\mathbf{Y}^T, \mathbf{B}^T\right) = \left(\mathbf{y}_1^T, ..., \mathbf{y}_N^T, b_1, ..., b_M\right)$, with $\mathbf{y}_j = (\mathbf{r}_{r,j}, c\delta_{r,j})$ for every epoch t_j.

The parameter vector is split in two; the $4N$ dimensional vector $\mathbf{Y}$ holding the receivers' position and its clock offset at each epoch, similar to the $\mathbf{H}$ matrix of SPP, but now for multiple epochs, and the M dimensional $\mathbf{B}$ vector containing the bias estimations. Hence, the total number of parameters to be estimated is $4N+M$, with N, the number of epochs and M the number of biases. Consequently, the normal equations form a $(4N+M)\times(4N+M)$ matrix, with quickly increasing dimensions if the number of epochs and the number of navigation satellites increase. Partitioning of the normal equations helps solving the problem in a much more computational efficient way. The method in [27] is followed below to solve the partitioned equations.

The design matrix $\mathbf{H}$ is split up in $\mathbf{H}_Y$, containing the modelled linearised observation partials with respect to the position and clock offset of the receiver, given by Equation 5 and $\mathbf{H}_B$, corresponding to the carrier phase ambiguities, shown in Equation 6. In the former, the partials of the modelled observation from transmitter s only relating to epoch t_j of that particular measurement are shown. The same holds for the partials of the modelled phase observation of transmitter s with respect to the bias parameter in Equation 2; the only non-zero entry is for bias parameter k corresponding to the observation from that particular transmitter at that particular epoch. Vector $\mathbf{e}$ in the first equation is given by Equation 4, similar to SPP. The position vector r^s is, again, obtained from the simulated ephemerides of the GNSS satellites. In weight matrix $\mathbf{W}$, every row corresponds to another observation, and since KOD uses different types of observations, the noise

variances and hence the observation weights vary per row.

$$\frac{\partial h^s_{r,j}}{\partial \mathbf{Y}} = \left(\mathbf{0}_1^T, \cdots, \mathbf{0}_{j-1}^T, (\mathbf{e}_r^s(t_j); 1)_j^T, \mathbf{0}_{j+1}^T, \cdots, \mathbf{0}_N^T\right) \tag{5}$$

$$\frac{\partial h^s_{r,j}}{\partial \mathbf{B}} = (\mathbf{0}_1, \cdots, \mathbf{0}_{k-1}, 1_k, \mathbf{0}_{k+1}, \cdots, \mathbf{0}_M) \tag{6}$$

[27] shows how the partitioned equations can be rewritten to Equation 7 and simplifies further to Equation 8 to obtain an LSQ equation that is solved to determine the estimation parameters.

$$\begin{pmatrix} \mathbf{H}_Y^T\mathbf{W}\mathbf{H}_Y & \mathbf{H}_Y^T\mathbf{W}\mathbf{H}_B \\ \mathbf{H}_B^T\mathbf{W}\mathbf{H}_Y & \mathbf{H}_B^T\mathbf{W}\mathbf{H}_B \end{pmatrix} \begin{pmatrix} \Delta\mathbf{Y} \\ \Delta\mathbf{B} \end{pmatrix} = \begin{pmatrix} \mathbf{H}_Y^T\mathbf{W}(\mathbf{z} - \mathbf{h}(\mathbf{Y}_0, \mathbf{B}_0)) \\ \mathbf{H}_Y^T\mathbf{W}(\mathbf{z} - \mathbf{h}(\mathbf{Y}_0, \mathbf{B}_0)) \end{pmatrix} \tag{7}$$

$$\begin{pmatrix} \mathbf{N}_{YY} & \mathbf{N}_{YB} \\ \mathbf{N}_{BY} & \mathbf{N}_{BB} \end{pmatrix} \begin{pmatrix} \Delta\mathbf{Y} \\ \Delta\mathbf{B} \end{pmatrix} = \begin{pmatrix} \mathbf{n}_Y \\ \mathbf{n}_B \end{pmatrix} \tag{8}$$

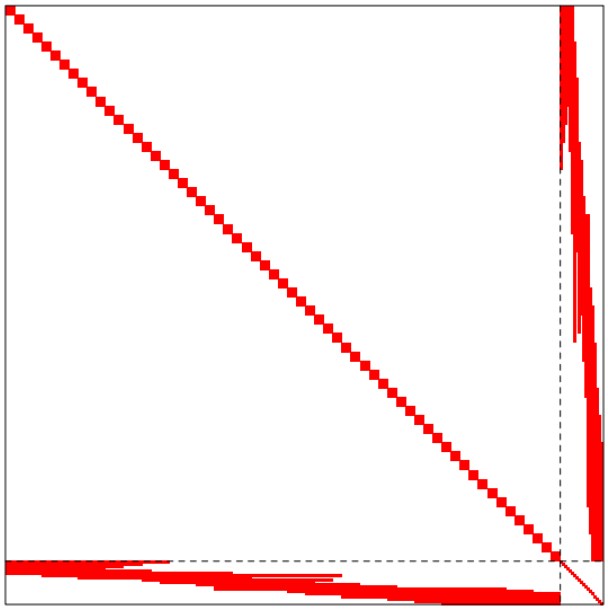

Figure 3: Figure 3.3 from [27]: "*Structure of the normal equations for kinematic least-squares batch estimation of epoch-wise position and clock corrections, as well as carrier phase biases over continuous tracking arcs*"

Figure 3 shows how the structure of the normal equations of a 1-hour data arc is visualised in his work. The structure of the $\mathbf{N}_{YB}$ and $\mathbf{N}_{BY}$ matrices, show that the positions and clock offsets are linked through the biases. Here, $\mathbf{N}_{BY} = \mathbf{N}_{YB}^T$, where $\mathbf{N}_{YB}$ is a $4N \times M$ matrix. The smaller block in the lower right corner corresponds to the $M \times M$ diagonal bias matrix, $\mathbf{N}_{BB}$. $\mathbf{N}_{YY}$ is a $4N \times 4N$ block diagonal matrix with 4×4 elements on the diagonal for every epoch. This sparsity is clearly visible in the large block in the upper left corner of the structure figure. The 4×4 matrices are similar to the normal matrices found in the SPP method. The difference here is that the phase measurements are included and, hence, the phase weights as well. Because of the sparsity of the matrix, the solution can be determined more efficiently. Besides that, the inverse of $\mathbf{N}_{YY}$ can be found by the relative simple inversion of the smaller sub-matrices on the diagonal. Kroes shows how to solve these equations efficiently by using the sparse character of the matrices and block elimination to find the parameter updates.

The estimation performs one calculation for every LPS satellite containing all of the N epochs. This calculation is repeated until the biggest parameter update is smaller than 10^{-8} m. A maximum of 5 iterations is maintained, the maximum update is below 1.5×10^{-8} m then, providing sufficient precision.

3.3.5. Inter-Satellite Linking

When ISL is applied, the observations between the LPS satellites are used in the estimation as well. Using these links in the estimation requires some rewriting of the algorithms.

This is because, in the first term of the observation equations, ρ_r^s, the transmitter, corresponding to superscript s, now is another LPS satellite. For a GNSS-LPS link the transmitter position is assumed to be known as the GNSS satellite broadcasts its position, while for ISL both the receiver and transmitter position have to be determined. The geometric range is dependent on $\mathbf{r}_r(t)$ and $\mathbf{r}^s(t)$, which both are parameters that have to be estimated. Hence, this problem can only be solved when the positions of both LPS satellites forming the link ends are estimated simultaneously. Because of the characteristics of the PECMEO constellation every LPS satellite is always in sight of any other LPS satellite; therefore, all nine LPS satellites are linked at any moment. Hence, to use ISL in the estimation, the positions of all the LPS satellites have to be estimated simultaneously. This leads to a parameterisation of the modelled observations with the position and clock offset of all the nine satellites, $\mathbf{y}_j = (x_{r1,j}, y_{r1,j}, z_{r1,j}, c\delta t_{r1,j}, \cdots, x_{r9,j}, y_{r9,j}, z_{r9,j}, c\delta t_{r9,j}) =$

$(\mathbf{r}_{r1,j}^T, c\delta t_{r1,j}, ..., \mathbf{r}_{r9,j}^T, c\delta t_{r9,j})$, at any epoch t_j. Per LPS satellite, denoted by the subscript r_n, four parameters, position and clock offset, are represented in this estimation parameter vector, giving a 36 dimensional vector.

To determine the design matrix $\mathbf{H}$ for the estimation scheme, the partial derivatives with respect to all these parameters have to be taken. That does not affect the modelled observations between the LPS and GNSS satellites, except for some extra zero entries. For the ISL observations, however, the design matrix contains partial derivatives with respect to the positions and clock offsets of both LPS satellites participating in the link. The position and the clock offset of both the receiver and the transmitter are thus estimated. Since multiple types of observations are introduced in this scheme, different weights appear on the diagonal of $\mathbf{W}$.

Following the method described for SPP, design matrix $\mathbf{H}$ now becomes a matrix with 36 columns. The number of rows is equal to the total number of observations done by every single LPS satellite. Note that in this matrix, every set of four columns represents a different LPS satellite with a different partial derivative corresponding to a parameter at every column.

From Equation 1, it becomes clear that when these partial derivatives are determined, the partial derivatives with respect to the receivers' parameters are the same as for standard SPP. The position partial derivatives create the line of sight unit vector $\mathbf{e}$ as in Equation 4, so the partial derivative with respect to the transmitters' position is the exact opposite of that of the receiver. The partial derivative with respect to the transmitters' clock offset is -1. This gives the partials of modelled measurement from LPS satellite r_3 to LPS satellite r_1 with respect to both their parameters and only relating to those two satellites as shown in Equation 9.

The equation shows that for ISL observations, the row in the design matrix contains eight non-zero entries, located in the columns corresponding to the two participating satellites. Rows representing GNSS observations remain to have four non-zero entries.

$$\frac{\partial h_{r_1}^{r_3}}{\partial \mathbf{y}_0} = \left(\left(\mathbf{e}_{r_1}^{r_3}; 1\right)_{r_1}^T, \mathbf{0}_{r_3}^T, \left(-\mathbf{e}_{r_1}^{r_3}; -1\right)_{r_2}^T, \mathbf{0}_{r_4}^T, \cdots, \mathbf{0}_{r_9}^T \right) \tag{9}$$

The normal matrix that is formed from the design matrix is 36×36. With this method, the different LPS satellites observations are thus correlated, but the epochs are still not linked.

Moving from SPPISL to KODISL by linking the epochs, to allow the use of measurements containing biases, the same similarities between SPP and

KOD as seen before are present. In the same fashion as the conversion of the SPP algorithm, the conversion of the KOD algorithm is explained.

As there are 36 parameters that have to be estimated per epoch and the biases for the phase observations, the total number of parameters to be estimated is $36N+M$. The complete normal matrix for the method would thus be a $(36N+M)\times(36N+M)$ dimensional matrix, which again would require a significant amount of computational effort for the inversion. However, the normal equations can be separated, in a similar fashion as described before, to create a problem that can be solved more efficiently. The parameter vector is split in a positions and clock offsets vector and a bias vector like before: $\left(\mathbf{Y}^T, \mathbf{B}^T\right) = \left(\mathbf{y}_1^T, \cdots, \mathbf{y}_N^T, b_1, \cdots, b_M\right)$, but now with $\mathbf{y}_j = (\mathbf{r}_{r_1,j}^T, c\delta t_{r_1,j}, ..., \mathbf{r}_{r_9,j}^T, c\delta t_{r_9,j})$, at any epoch t_j.

The normal equations are partitioned in the same way, and Equation 8 is used to obtain the LSQ updates for the parameters, but the matrices have different dimensions. Again, $\mathbf{N}_{YY}$ matrix is obtained by taking only the partial derivatives with respect to the satellites' positions and clock offsets into account, but now for the nine LPS satellites simultaneously. Hence, it is a $36N\times36N$ block diagonal matrix, containing 36×36 blocks which are similar to the SPPISL normal matrices. In the KODISL 36×36 matrix, weights for different measurement types are involved as also phase observations are included. This difference is similar to the difference between the KOD $\mathbf{N}_{YY}$ matrix and the SPP normal matrix. The normal matrices $\mathbf{N}_{YB}$ and $\mathbf{N}_{BY}$, connecting all the positions and clock offsets through the biases, are a $36N\times M$ dimensional matrix and its transpose, respectively. $\mathbf{N}_{BB}$, which is solely based on the partial derivatives with respect to the biases, is an $M\times M$ matrix.

The partial derivatives found in the normal matrices are found with Equation 10 and Equation 11 and Equation 12 for the positions and clock offsets and the biases, respectively.

$$\frac{\partial h_{r1,j}^{r3}}{\partial \mathbf{Y}} = \left(\mathbf{0}_1^T, \cdots, \mathbf{0}_{j-1}^T, \left(\frac{\partial h_{r1,j}^{r3}}{\partial \mathbf{y}_j}\right)_j^T, \mathbf{0}_{j+1}^T, \cdots, \mathbf{0}_N^T\right) \tag{10}$$

where,

$$\frac{\partial h_{r_1,j}^{r_3}}{\partial \mathbf{y}_j} = \left(\left(\mathbf{e}_{r_1}^{r_3}(t_j); 1\right)_{r_1}^T, \mathbf{0}_{r_3}^T, \left(-\mathbf{e}_{r_1}^{r_3}(t_j); -1\right)_{r_2}^T, \mathbf{0}_{r_4}^T, \cdots, \mathbf{0}_{r_9}^T\right) \tag{11}$$

$$\frac{\partial h_{r_1,j}^{r_3}}{\partial \mathbf{B}} = (\mathbf{0}_1, \cdots, \mathbf{0}_{k-1}, 1_k, \mathbf{0}_{k+1}, \cdots, \mathbf{0}_M) \tag{12}$$

The first two equations give the partials of modelled measurement from LPS satellite r_3 to LPS satellite r_1 with respect to both their position and clock offset parameters and only relating to those two satellites. The equation shows the number of zero entries in the equations that causes the matrix to be so sparse. Equation 12 shows that the only non-zero elements corresponds to the bias for the observation between the satellites at that particular epoch. The inversion of $\mathbf{N}_{YY}$ can be carried out by finding the inversions of the 36×36 sub-matrices on the diagonal.

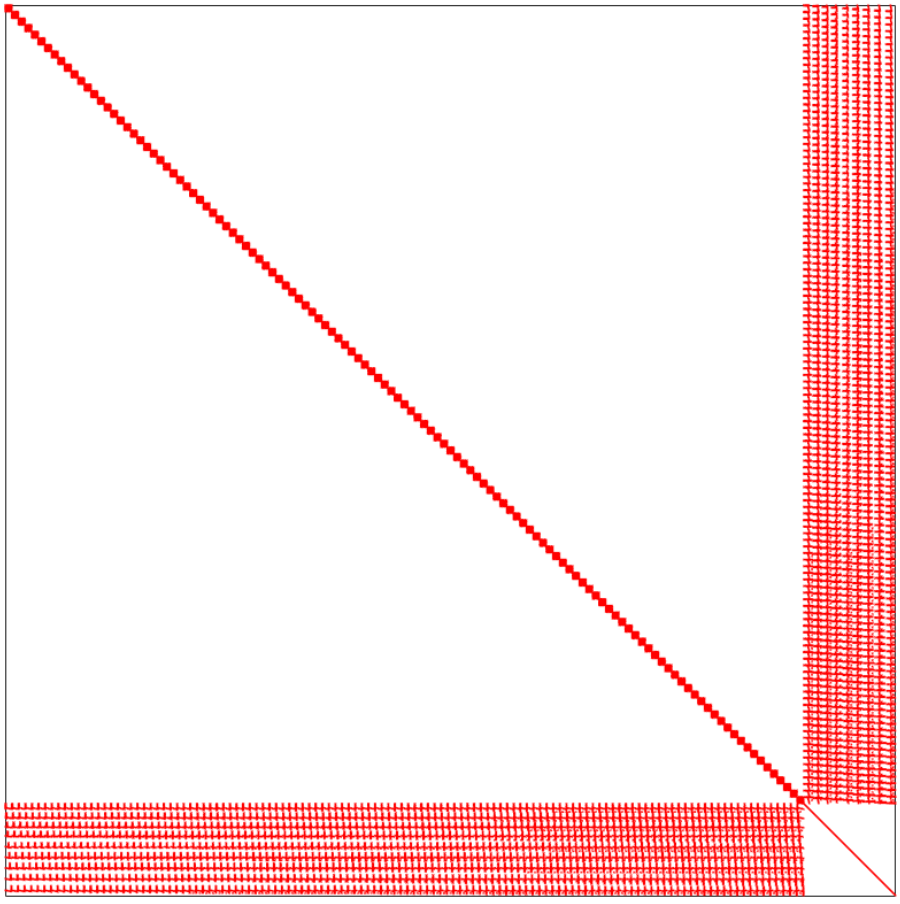

Figure 4: Structure of the normal equations for kinematic least-squares batch estimation of epoch-wise position and clock corrections, as well as carrier phase biases over continuous tracking arcs for nine interconnected satellites

Following these modifications, the general structure of the normal equa-

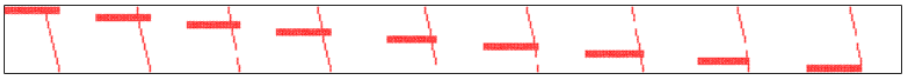

Figure 5: Structure of N_{XB} for one epoch in 1-hour data arc

tions from Equation 8 for the KOD ISL algorithm is visualised in Figure 4 for a 1-hour data arc. Comparing this figure with Figure 3 from the existing KOD algorithm, there are some clear similarities, such as the sparsity of N_{YY} and N_{BB}. The diagonal of the former, however, now contains the 36×36 matrices. The N_{XB} and N_{BX} matrices are much more populated, this is because the biases of the measurements of nine satellites are shown. Besides that, the ISL observations interconnect the position and clock offsets of separate LPS satellites. Figure 5 shows the structure of N_{XB} of one epoch. The biases of the different satellites and the ISL biases are clearly visible.

3.3.6. Clocks in Phase

Another envisioned capability of the LPS is the ability to have the clocks of the various satellites in phase, as stated in Section 2. This way, only one clock has to be estimated per epoch instead of nine separate clocks, so fewer parameters to be estimated, which in general leads to a higher accuracy estimation of the leftover parameters. This approach is only used for KODISL as the other algorithms are merely used to get initial estimates for KODISL. The approach is very similar to the methods described before, so only the most important features and differences are stated. The positions and clock offsets parameter vector takes on the form of $\mathbf{y} = (x_{r_1}, y_{r_1}, z_{r_1}, ..., x_{r_9}, y_{r_9}, z_{r_9}, c\delta t_{r*}) = (\mathbf{r}_{r_1}^T, ..., \mathbf{r}_{r_9}^T, c\delta t_{r*})$. Here the subscript $r*$, denotes the clock offset of the synchronised system clock. The design matrix now has 28 columns for the positions of all nine satellites and the shared clock offset estimates per epoch and M additional columns for the biases to be estimated for this method. The normal equations again are divided into four separate matrices; now the N_{YY} matrix is a block diagram matrix with 28×28 sub-matrices on the diagonal. An important difference with the other algorithms is that when the clocks are in phase, one clock offset is estimated for the entire system, this means that for the modelled observations between the LPS satellites the receiver and transmitter clock offsets cancel out according to Equation 1 and Equation 2. Hence, the clock offset entries in the design matrix for the LPS-to-LPS measurements are equal to zero.

In Table 2, the different dimensions for the several matrices and vectors

Element	SPP	KOD	KODISL	KODISL 1 Clock
$\mathbf{y}$	4	$4N+M$	$36N+M$	$28N+M$
$\mathbf{H}$	$m\times4$	$m\times(4N+M)$	$m\times(36N+M)$	$m\times(28N+M)$
$\mathbf{N}$, $\mathbf{N}_{YY}$	4×4	$(4N+M)\times(4N+M)$	$(36N+M)\times(36N+M)$	$(28N+M)\times(28N+M)$
$\mathbf{N}_{YB}$, $\mathbf{N}_{BY}^{T}$	-	$(4N+M)\times M$	$(36N+M)\times M$	$(28N+M)\times M$
$\mathbf{N}_{BB}$	-	$M\times$M	$M\times M$	$M\times M$

Table 2: The dimensions of the different matrices and vector that occur in the various estimation techniques

required in the tool are given.

3.3.7. Different System Configurations

The beginning of this section states the different system configurations for the ISL technique and error cases. This subsection gives their implications for the estimation algorithms, starting with the system configurations.

The GNSS-like ISL system does not require any changes other than the ISL algorithms described above. Considering the LRI system, one should realise that this is a range type measurement and, thus, treated as a GPS code measurement. No bias has to be estimated so the weight of the phase measurements is set to zero in the algorithms. This way only the absolute range observations are considered. The K-band ranging is a phase-type measurement, requiring biases to be estimated, but there is no direct range type measurement. Hence, the code weight is set to zero in order to simulate the absence of range observations. A range measurement is still simulated to obtain an initial estimate for the biases, which is determined by using the difference between the range and the phase measurement. The accuracy of this code measurement is based on the position estimation accuracy of the algorithms executed before moving to ISL; SPP and KOD per satellite.

Regarding the different error cases, the two separate sources that this study considers are included in different ways. The measurement noise with a random error function is simply added to the measurements during the simulation as Subsection 4.3 shows. The systematic ephemeris errors are added during the estimation process, when the modelled observation is determined in the algorithms. This is done by calculating the modelled geometric range as the difference between the receiver and the transmitter position. However, now an error on the broadcasted position of the transmitter is simulated by adjusting its Semi-Major Axis (SMA). This is explained in more detail in Subsection 4.6.

It is essential to note that the weights of the observations are held constant

for different simulation cases. For every simulation case the inverted variance of the supposed accuracy of the noisy measurements is used to determine the weights of the measurements ($\mathbf{W}_i = \sigma_i^{-2}$). For the noise-free simulations, where in reality the variances are equal as a result of the absence of noise, the same noisy weight values are used.

3.4. Execution

With the developed algorithms, the positions of the LPS satellites can be estimated using different system configurations and error sources. In theory, the algorithms that use the most measurements are the most accurate, and it is expected that KODISL will provide the most precise results. However, since the positions of the LPS satellites are used in this algorithm, the solutions may require many iterations or can even be diverging and become very inaccurate if the initial estimates are not precise enough. For this reason first SPP, followed by KOD, will be applied to get initial positions for the satellites. This way, the iteration process is computationally less expensive as less iterations are required for convergence. This is also the reason why, in practice, SPPISL is not used for the estimation. When only SPP is executed beforehand, the a priori estimates are not accurate enough for position estimations including ISL as described above. On the other hand, when ISL observations are included, it is preferred to use all the measurements available, so also the phase measurements, to constrain the problem as much as possible, hence the KODISL algorithm is used instead of SPPISL.

4. Simulation Environment

This section describes the simulation setup, including the Earth environment, the GNSS modelling, the error sources incorporated, and the assumptions made. It defines the environment where the simulations are done in and describes how the simulations are done to obtain the products to carry out the methodology described earlier. The section treats the two blocks in the top of Figure 2 as well as the ephemeris error generation.

4.1. Dynamical Model

In the design of the PECMEO system, it is assumed that the effect of perturbations from third bodies (the Moon mainly), solar wind, satellite temperature gradient, atmospheric drag and other sources can either be corrected through propulsion or is tolerated or even negligible over the mission

duration [29]. In addition, the orbital altitude is chosen in such a way that atmospheric effects are avoided as much as possible [20].

Besides that, it is important to realise that in this phase of the lunar navigation system design the main goal is to show the promising capabilities of a Lunar Positioning System consisting of a PECMEO constellation and the incorporation of ISL in particular. The inclusion of an extremely detailed dynamical model it is not necessary to prove this.

Therefore it was chosen that this study limits itself to Kepler orbits for propagation of the satellite states. This way the satellites are only accelerated by the gravity of the main body they are orbiting, the Earth, which is described by a point mass. The study considers no other perturbations at this point. The simulation of the LPS satellites and the GNSS constellations makes use of a so-called low fidelity dynamical model.

4.2. Orbit Simulation

Since all the orbit propagations are described with Kepler orbits, only the initial Kepler elements and propagation epochs are required to simulate the orbits. Because of the low fidelity force model, this work considers no interactions of other planets. Hence, the reference frame orientation does not have an impact on the desired results. J2000 is used as start epoch.

4.2.1. LPS Simulation

The LPS is a PECMEO constellation, which is described before, but here a slightly more detailed description is given about the orbits. The first plane is the equatorial plane, and the satellites are evenly distributed over the orbit, that means the satellites are positioned at 0°, 120° and 240° in the argument of periapsis (ω) - or in true anomaly as there is no perigee in the circular orbit, making $\omega = 0°$. The second and third plane are both polar, so their inclination is set to 90°. To make the planes perpendicular to each other, the third plane has its longitude of the ascending node set to 90°, while this is 0° for the second plane. In these planes, the satellites are also evenly distributed, similar to the first plane. Like mentioned before, circular orbits are used, so the eccentricity is zero, and the semi-major axis is 14,000 km for all satellites. Note that when for the second plane the inclination is increased, the plane rotates about the axis pointing to the first satellite. This rotation results in the same location for the first satellites, at 0° true anomaly, of the first and second orbital plane. Therefore, the satellites in the second plane are given a small offset of 5° to avoid collisions. Hence, their

initial true anomaly angles are 5°, 125° and 245°. An important note is that the PECMEO constellation is not optimised as part of this study as it purely focuses on the position estimation capabilities and performance.

4.2.2. GNSS Simulation

The GNSS constellations are simulated as Walker Delta Pattern constellations, this means that t satellites are evenly divided over p circular orbits at an inclination i with f as the relative spacing between satellites in neighbouring planes. This gives the notation: *i: t/p/f*. The change in true anomaly (in degrees) for parallel satellites in adjacent planes is equal to $f \times 360/t$, in this simulation that change, and thus f as well, is equal to zero. Within the circular orbits, the satellites are uniformly distributed over 360° [39]. In this last point, GPS is an exception, where the angular difference between the satellites in each orbital plane is 30°, 105°, 120°, and 105° apart [40]. Apart from this exception, the four GNSS constellations included in this study are simulated according to the following Walker notations and altitude:

- Galileo, 56°: 30/3/0 at 23,222 km
- GLONASS, 64.8°: 24/3/0 at 19,100 km
- BeiDou, 55.8°: 27/3/0 at 21,500 km
- GPS, 55°: 30/6/0 at 20,200 km

This work simulates the constellations for a period of one day with time steps of 30 seconds, giving 2881 epochs. The LPS satellites orbit the Earth more than five times and the GNSS satellites approximately two times in this time. This period is assumed to give enough insight into the performance of the satellites and the geometric distribution of the different constellations. A simulation period of one day is typical for orbit determination problems around Earth, besides, longer simulation times would significantly increase the computational effort required.

4.3. Observation Simulation

This subsection explains how the simulator produces the observations used in the estimation process. It also discusses the appearance of a navigation observation. To produce the observations that the estimation process uses, it should be known what a navigation observation looks like. This study recognises two types of observations, unambiguous observations that represent a (pseudo-)range between two points, which can be used directly, and observations that require the estimation of an ambiguity in order to be used.

These two types of observations are referred to as range measurements and phase measurements, respectively. GPS pseudorange code observations and GPS carrier phase observations are examples of the two types. Following [27], a GPS pseudorange code observation and GPS carrier phase observation from transmitter s to receiver r are described by Equation 13 and Equation 14.

$$P_r^s(t) = \rho_r^s(t) + c(\delta t_r(t) - \delta t^s(t - \tau_r^s(t))) + I_r^s(t, f) + M_{rP}^s(t) + \epsilon_{rP}^s(t) \quad (13)$$

$$L_r^s(t) = \rho_r^s(t) + c(\delta t_r(t) - \delta t^s(t - \tau_r^s(t))) - I_r^s(t, f) + \lambda A_r^s + M_{rL}^s(t) + \epsilon_{rL}^s(t) \quad (14)$$

In these equations ρ_r^s is the geometric range from transmitter satellite s to receiver satellite r, c is the speed of light, δt is the clock offset of either satellite and τ_r^s is the true signal travelling time between the satellites. I_r^s represents the ionospheric path delay, ϵ_r^s is the measurement noise of the observation type, λA_r^s is a representation of the integer ambiguity and M_r^s denotes all other (systematic) errors.

As mentioned before, this study limits itself to two different error sources, namely the measurement noise and the ephemeris error. Other errors are not considered and therefore assumed to be zero. Some of the more significant error sources appearing in the equation are shortly discussed in the following.

The clock offset error is the incorrect time at a satellite and its drift over time, errors like this can play a significant role and are interesting to investigate in later studies.

The ionospheric path delay is not considered in this study. Because of the envisioned orbital altitude at which atmospheric effects are largely avoided, this error source is less relevant for the LPS application, while it can be the most significant source of errors in many GPS applications.

The measurement noise of the observation type, describes the accuracy of the measurements of that particular observation type. This is one of the two error sources included in the simulations. The noise is assumed to be completely random with a zero mean and for the large number of observations, the noise error is simulated with a normal distribution with zero mean as per the central limit theorem. The estimated accuracy of the measurement gives the standard deviation used. This value differs per observation type and is discussed in more detail in Subsection 4.5. In general, the noise level is much lower for phase measurements. Therefore it gives better results provided that the ambiguity is solved for. The value of the measurement noise is different for every single observation. In reality, the measurement noise

does not have a constant standard deviation but is dependent on different parameters; however, other noise models are beyond the scope of this study.

The M_r^s term usually denotes a collection of smaller and lower order errors and is for this study completely omitted. Note that the systematic error induced by the GNSS ephemeris error, however, is included in the simulations. It is not applied to the observation, though, but differently, as described in Subsection 4.6.

The ambiguity is an integer number of carrier cycles which is approximated by a float value to obtain a range from the phase measurement. The integer ambiguity is a number that is constant for the entire duration of a link between a receiver and a transmitter, when the signal is blocked or lost between the two and later retrieved, a different number has to be estimated. The wavelength λ is dropped from the term and an integer number of meters is simulated for the bias.

Subsection 4.4 gives an additional explanation of why this study does not consider the Light-Time Correction (LTC). So τ_r^s is equal to zero, and the geometric range is the actual distance between the two simulated points in the Kepler orbits of the two satellites between which the observation is.

This means that the equations used to simulate the observations for this research are reduced to Equation 15 and Equation 16. The simulated signals only consist of the geometric range and the measurement noise of the observation system and, in case of a phase measurement, also an ambiguity.

$$P_r^s(t) = \rho_r^s(t) + \epsilon_{rP}^s(t) \tag{15}$$

$$L_r^s(t) = \rho_r^s(t) + A_r^s + \epsilon_{rL}^s(t) \tag{16}$$

For an observation between receiver r and transmitter s at epoch t_j the geometric range is taken directly as the norm of the vector between the position of the receiver $\mathbf{r}_r(t_j)$ and the position of the transmitter $\mathbf{r}^s(t_j)$ at that instant. The noise error at that epoch is randomly generated with a normal distribution, mean zero and standard deviation corresponding to the measurement type. For the simulation of the ambiguity, the simulation tool first checks if an observation between r and s was present at the previous epoch t_{j-1}, if this is true that same ambiguity is used. Otherwise, a number of carrier cycles is randomly generated between -10,000 and 10,000 m.

All the observations occurring in this study use the two derived simulation equations. All the range type measurements use the first equation, so

the code measurements between GNSS and LPS satellites and in between LPS satellites for the first ISL system configuration, but also the LRI ISL measurements use it. The simulator uses Equation 16 to simulate carrier phase measurements between GNSS and LPS satellites, phase measurements of GPS ISL system and KBR observations for ISL.

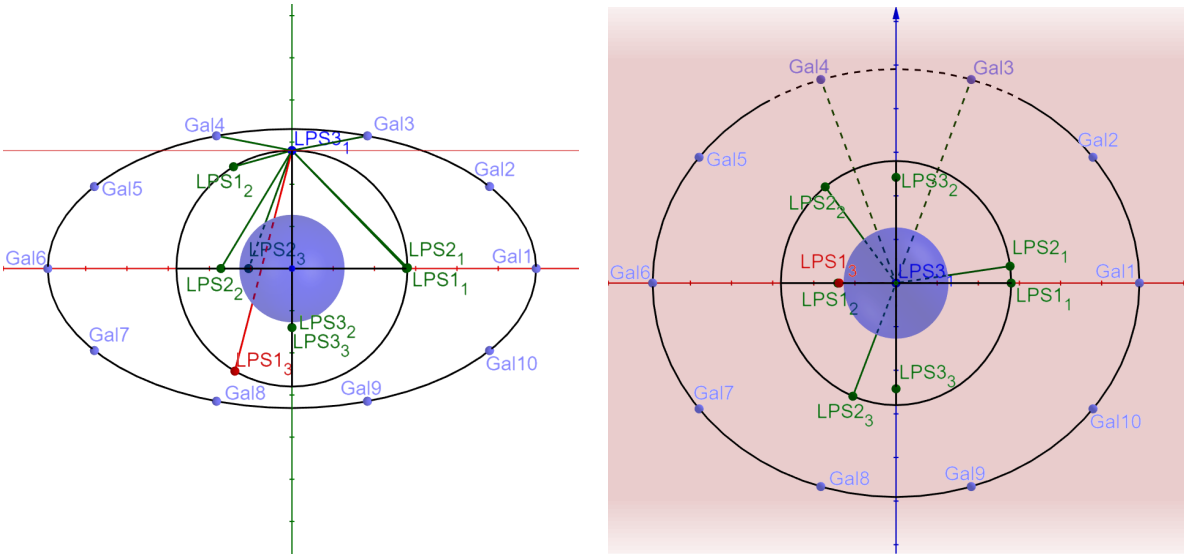

(a) Top view

(b) Side view from y-axis

Figure 6: Top and side view on the LPS constellation and one orbital plane of Galileo

4.3.1. Observation Visibility

These observations can only be done when a link can be established between two satellites, that is, when two satellites are in each others Field of View (FoV). The first important factor that blocks the field of view of the satellites is the occultation of the Earth, when part of the Earth lies between two satellites, the line of sight is blocked, and no observation is possible.

Besides that, there is the field of view of a satellite, in this context determined by the measurement instrument and its direction. This study assumes that the communication between LPS satellites and GNSS satellites is only possible if the GNSS satellite lies above the LPS satellites' local horizon. In other words, the elevation angle has to be bigger than zero with the local horizon of the satellite as reference. This corresponds to a semi-omnidirectional GPS receiver antenna pointing outward, away from the Earth.

ISL observations between the LPS satellites can be done in any direction, as long as the Earth does not block the signal. Since the altitude of all LPS satellites is equal, this effectively means that the signals always come from the side pointing towards the Earth. Therefore only a semi-omnidirectional receiving and transmitting antenna pointing toward the Earth is required.

Figure 6a to Figure 7b depict the LPS constellation and one orbital plane of the Galileo constellation along with the possible links (green) from an LPS satellite in one of the polar planes. There are links possible with two different Galileo satellites, Gal_3 and Gal_4, because the limited view of which the red plane indicates the edge. Links with seven of the eight other LPS satellites are possible, with the exception denoted as $LPS1_3$, because of the occultation of the Earth.

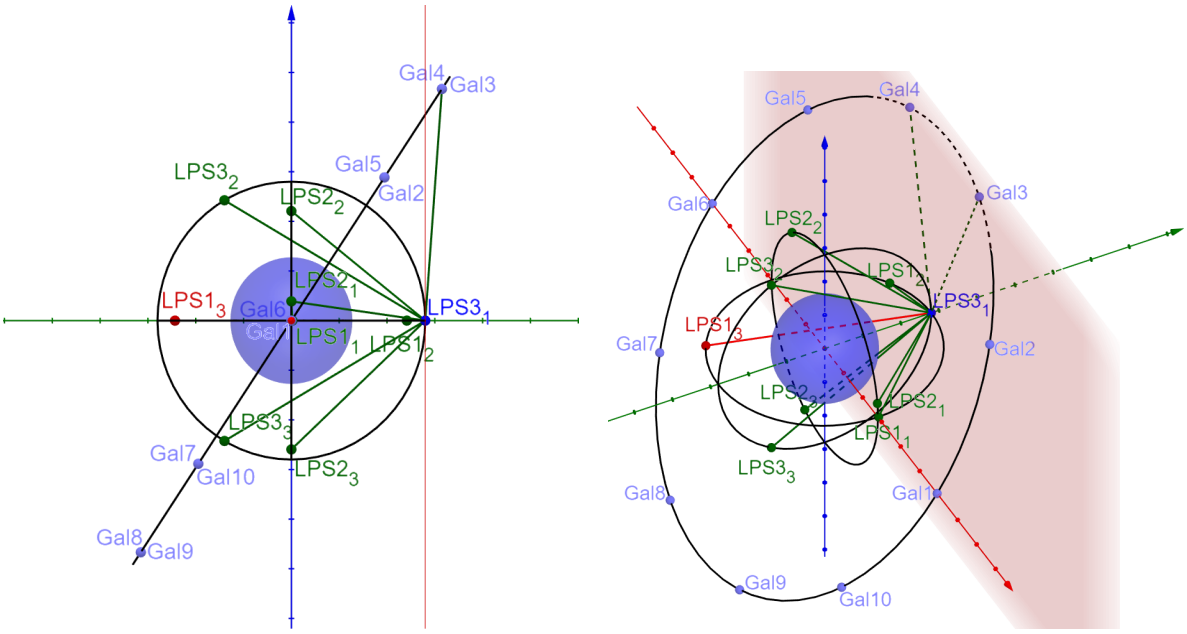

(a) Side view from x-axis

(b) Tilted view

Figure 7: Side and tilted view on the LPS constellation and one orbital plane of Galileo

In reality, the communication instruments grant no semi-spherical view, because antennas can have elevations masks and the LRI system requires directed reflectors to perform measurements. This is something to consider for the expansion of the tools when the model becomes more realistic.

4.4. Light-time Correction

The LTC can be used to get more realistic simulations. The correction is based on the fact that the transmission of the signal between two satellites is not instantaneous, but happens with the speed of light. This means that the measured distance between two satellites is in reality slightly larger or smaller as the transmitter moves in the time that the signal needs to travel from the transmitter to the receiver. Tudat has a built-in LTC tool that makes use of an iterative process to find the correct measured (pseudo-)range. The true travel times can also be obtained. In the estimation process, the travel times can be used to correct the epoch for the transmitter in order to obtain the appropriate GNSS position corresponding to the corrected range measurement from the Kepler ephemeris.

When ISL is used, however, using the LTC causes trouble, because the LPS positions are being estimated and no ephemeris is available. The dynamics of the satellites are unknown since only SPP and KOD are executed, and the Kepler elements can not be determined. Hence, the position at the corrected epoch can not be determined. Using the corrected range measurement would cause inconsistencies in the estimation. It is decided to neglect using the correction in this study as applying LTC on the ISL system proves to be challenging and beyond the scope of this study. In future research, when additional estimation schemes are being used and dynamics are also estimated, LTC can be incorporated more straightforwardly. Another option for future work, is to modify the KOD algorithm to incorporate the LTC.

Also, incorporating the LTC in KOD without ISL observations causes a minimal impact. The maximum difference in the absolute position error is only 5.1910×10^{-8} m in the noise-only case and 1.7483×10^{-6} m in the combined error case if the LTC is integrated. The differences are negligible, thus it is fair to assume that the results based on including ISL and no LTC are still representative and that extending the KODISL for including the LTC will not lead to different conclusions. Hence, the LTC is not included in the simulation for this study.

4.5. Measurement Noise

GNSS Noise

For the observations received from the GNSS constellations, the LPS satellites use a standard GPS receiver. The standard deviations of the measurement noise are $\sigma(\epsilon_P) = 1$ m and $\sigma(\epsilon_L) = 1$ mm for code and carrier phase

measurements, respectively [41]. Thus, the weights for the GNSS observations are 1 and $1{\times}10^6$, for every simulation case.

ISL Noise

For the links between the LPS satellites themselves, the type of measurements is yet to be determined. For this reason, this study compares multiple system configurations. This work recognises the GPS-like system option and the much more precise LRI and KBR options, discussed below.

GPS ISL - The first system configuration is based on instruments comparable with conventional GNSS satellites, this way the LPS constellation acts as an additional GNSS system. With this configuration, the inter-satellite link produces code measurements with 1 m noise and carrier phase measurements with 1 mm noise as standard deviations, just as described for the GNSS segment. The observations also have the same weights as for GNSS.

LRI ISL - The second system applies a laser ranging technique that is also used in the GRACE Follow-On mission to determine the relative distance between its two satellites with extreme accuracy [37]. The technique provides unambiguous pseudorange measurements. Therefore its observations are simulated in the same way as GNSS code measurements, but with much smaller noise levels. In reality, LRI can provide measurements with noise reaching the nanometre level. However, the simulations in this study are limited by the precision of the system used. As the simulation and the computations are performed with 64-bit real numbers, numbers are limited to 15 to 16 digits. The relatively large orders of magnitude for the distances between satellites compared to the small orders of magnitude for the noise levels play a significant role in the limitations of the precision. The longest distance between two LPS satellites in sight of each other is about 25,000 km or 2.5×10^7 m. This means that the computer rounding error appears at approximately $1{\times}10^{-9}$ m, at the nanometre level. Therefore it makes no sense to simulate errors with a standard deviation in this order of magnitude as the error is indistinguishable from the computer rounding error.

Besides that, it was shown that the algorithms are not able to converge anymore and even diverged in most cases if standard deviations lower than $1{\times}10^{-7}$ m are used. The algorithms developed for this study are not correctly compatible with such low standard deviations and the corresponding extremely high weight levels obtained through $W_i = \sigma_i^{-2}$. This is due to high accuracy laser weights of $1{\times}10^{16}$ that are mixed with weights of 1, for the GNSS code observations. This combination causes large numerical instabilities in the matrix calculations as the condition number of the normal

matrix goes up to the order of magnitude of 10^{10}. With a condition number this high, there is a risk of losing ten decimals in the solution, leading to extremely inaccurate calculations. Besides that, this combination of weights conflicts with the computer precision.

Therefore, the LRI measurements are simulated with a standard deviation of $\sigma(\epsilon_{LRI}) = 1{\times}10^{-7}$ m. This is a conservative, but still extremely precise, assumption as in reality the measurement may be more precise. A computer system with a higher precision is required to allow for such simulations. Also, adjustments in the mathematical routines would be required to take care of the numerical stability and handle the condition number. With the selected noise level, the weight for LRI observations is $1{\times}10^{14}$ (and 0 for the phase observations as they do not exist); this applies for all simulation cases.

KBR ISL - Another measurement system used to achieve much higher precision is the KBR instrument, as is used in the original GRACE missions [25]. GRACE was able to provide biased range measurements with a noise level of 10 μm at 1 Hz sampling [42]. The technique is already proposed for the ISL of PECMEO satellites and for such satellites, the range accuracy of 32.3 μm is calculated [30]. Hence, this study takes $\sigma(\epsilon_{KBR}) = 3 \times 10^{-5}$ m for the standard deviation of the noise of KBR observations. The downside of this type of observations is the need to estimate a bias for every link arc between two LPS satellites. To obtain an initial estimate for this bias, the KBR observation is subtracted from an a priori relative distance measurement. For traditional GNSS measurements, the code measurement is used, but for KBR, only a phase measurement is available. However, since the ISL algorithms are only performed after execution of SPP and KOD algorithms, the results from those estimators should be used to perform the estimation. In this study, this a priori result is simulated by generating a code-like measurement with zero weight and a standard deviation of 0.5 m, approximately two times the biggest estimation error after the KOD estimator. This way, the measurement is not used in the estimation, but it does provide a way to determine an initial guess for the bias. The universal weights for the observations of KBR are 0, as there is no range measurement, and $1.1{\times}10^{9}$.

4.6. Ephemeris Error

The methodology section explains that, for the observations between GNSS and LPS, the ephemerides of the GNSS satellites is used to determine the positions of these satellites at particular epochs in order to perform the estimation schemes.

The broadcast ephemerides of the GNSS constellations hold the Kepler elements of orbits where the satellites currently are assumed to be in. In reality, the GNSS orbits are not perfect Kepler orbits, which make the satellites to drift from the ephemeris. The ephemerides have to be updated to determine new Kepler elements that describe the orbit of the satellite for a period of time, referred to as ephemeris arc. The Kepler elements determined at the beginning of that ephemeris arc are used to find the position of the satellite at a particular epoch within this ephemeris arc. This is where the ephemeris error is induced as the observation from a transmitter and the predicted position of the transmitter do not match. In orbit determination, the ephemeris error of navigation satellites have a massive impact on the total positioning error [26].

This study assumes that the ephemerides of the GNSS satellites are updated every half hour, which leads to a series of 48 distinct Kepler orbits starting at each update epoch.

Because the GNSS ephemerides are simulated using Kepler orbits, there is no error in the predicted orbits. Hence, the ephemeris error has to be simulated for every ephemeris arc. At the beginning of each arc, the Kepler orbit is determined and disrupted, the deviated Kepler orbit is used to determine the position of the satellite on a desired epoch within the arc. The disruption, that represents the inaccuracy in the estimated GNSS Kepler orbit, is a small deviation added to the semi-major axis (SMA).

The absolute error of the GNSS position increases over time following the incorrect Kepler orbit, and at the end of the ephemeris arc, the ephemeris is updated. The update consists of a correction of the Kepler orbit and the inclusion of a new SMA deviation for the following ephemeris arc.

The ephemeris error is only generated for the GNSS satellites. The positions of LPS satellites are being estimated, and the initial guess of a satellite is used as its transmitter position.

The SMA deviation is a randomly generated value between -10 and 10 cm this way the average error in the 3D position of the GNSS satellites is about 5 cm, which is a good approximation for a post-facto ephemeris error. With this deviation for the SMA and an ephemeris arc of 30 minutes, the absolute 3D position error does not get more than ten per cent bigger than the initial deviation, giving a 11 cm maximum position error. In reality, the update frequency of the GNSS ephemerides is lower, thus, the expected position of GNSS satellites is worse than assumed in this study, especially when real-time position information is required.

Simulations show that if the model only includes the ephemeris error, the estimation errors scale almost perfectly with the used standard deviation of the SMA. The decimetre deviations result in an average absolute 3D position error of some centimetres, while the centimetre deviations result in millimetre position errors, so a tenth of the deviation is proportional to the caused the error. Along these lines, when the ephemeris error is a metre, the absolute position error is about ten times bigger than for the decimetre ephemeris error. When noise is also considered in the model, the proportions are different, and the centimetre deviations cause errors that are slightly larger than a tenth of the decimetre deviation. This is because the noise error gets a more substantial influence on the estimation as the ephemeris error decreases.

5. Results

This section presents the results found by following the methods explained in Subsection 3.3. The difference between the true simulated position and the estimated position gives the position error for a system configuration. The study considers the position error average of the nine LPS satellites as the accuracy of the system configuration as shown in Equation 17. The equation gives the error per epoch j, where $\Delta x_{i,j}$ denotes the difference between the true and the estimated x-coordinate of satellite i at epoch j.

$$error(t_j) = \frac{1}{9}\sum_{i=1}^{9}\sqrt{(\Delta x_{i,j})^2 + (\Delta y_{i,j})^2 + (\Delta z_{i,j})^2} \tag{17}$$

Separate figures show the results for the different sources of error. Every graph includes the seven different configurations of the system. The graphs also show the one day average of the position errors, found with Equation 18, in the legend. Table 3 at the end of this section lists these one day average errors to give a good overview of the different system performances.

$$average\ error = \frac{1}{2881}\sum_{j=1}^{2881} error(t_j) \tag{18}$$

5.1. Error-free Simulation

Figure 8 presents the results of the error-free observations solution. The figure shows that the majority of the estimation errors (94%) lies below $1{\times}10^{-8}$ m. Following the precision discussion in Subsection 4.5, this error

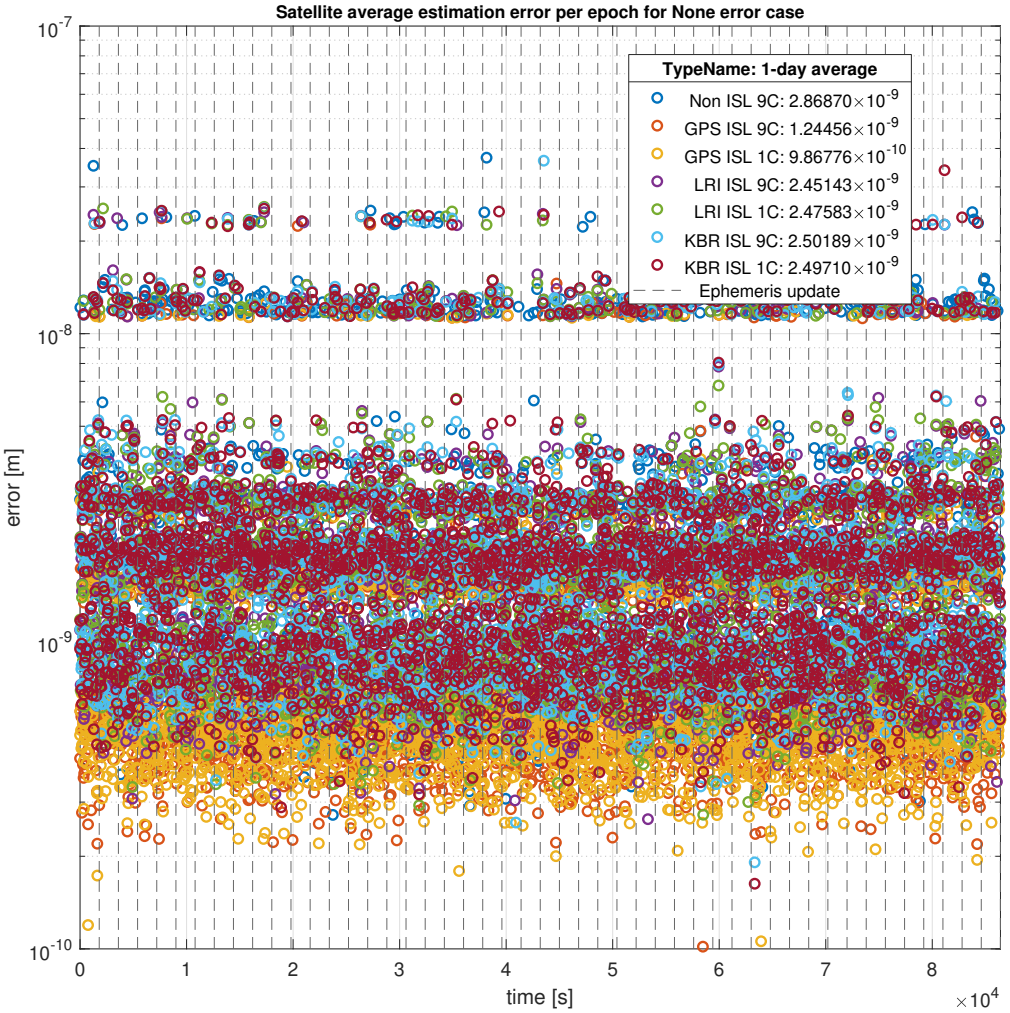

Figure 8: Satellite average of the LPS 3D position error over time when no errors are included

level indicates that the computer rounding error causes the error found since the 3D position of each of the satellites is about 1.4×10^7. Hence, the results are not very expressive, but give some basic insights.

The least accurate results are obtained if only GNSS measurements are used. When an ISL system is added, the estimation errors decrease, this is because geometric distribution is improved and because there are more observations to include in the estimation algorithm. The latter also explains why the LRI and KBR configurations provide worse average errors than the

GPS ISL system. These configurations either use pseudorange measurements or phase measurements, while GPS ISL provides a combination of these measurements, leading to twice as many extra observations.

Besides this, the results mainly prove to be proper verification of the estimation tools. The results show near-perfect estimations which is expected as no errors are added to the system, and only a rounding error is present.

5.2. Measurement Noise-only Simulation

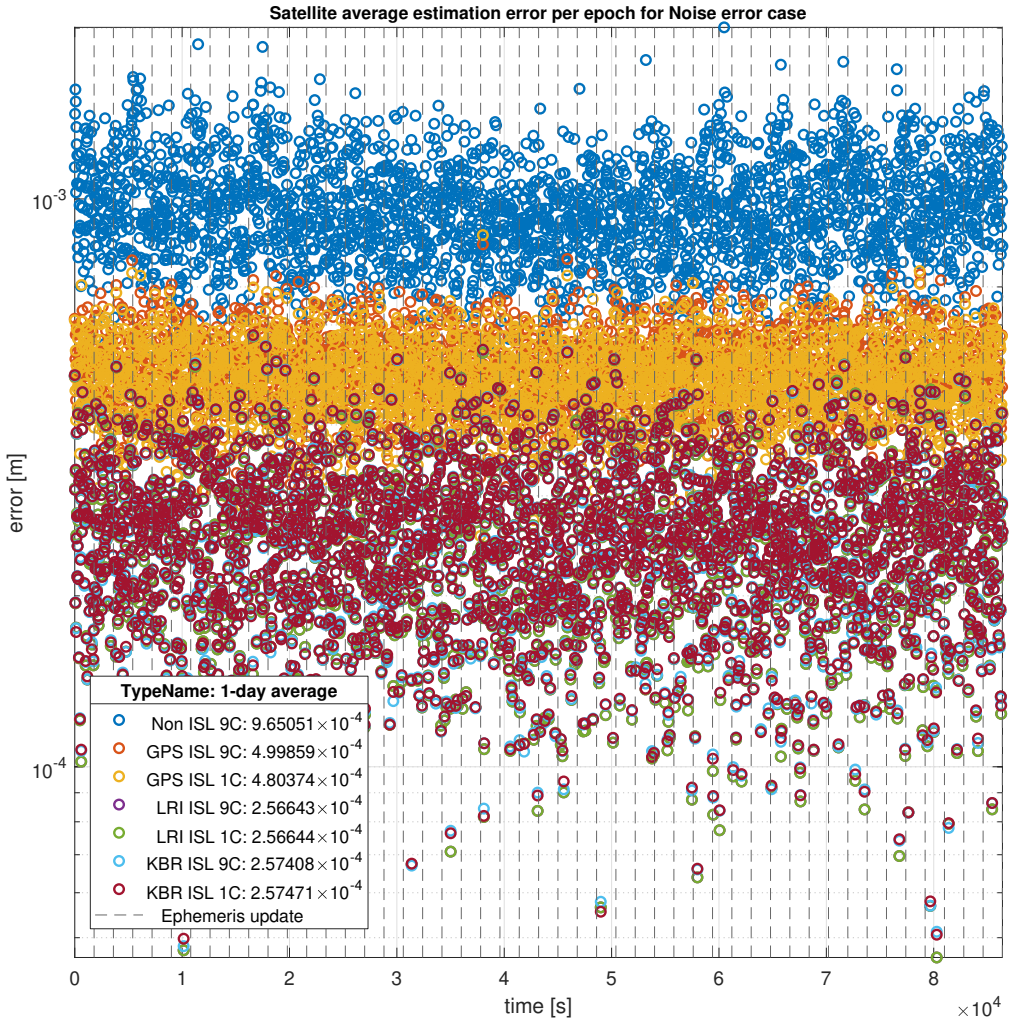

Figure 9: Satellite average of the LPS 3D position error over time if only noise errors are included

The first step in increasing the model complexity and the realism of the solution is including the measurement noise errors in this study. Figure 9 shows the estimated position error results for the case when the measurements include noise. It is evident that including the ISL measurements gives a significant improvement to the estimation of the LPS satellites' positions as three distinct bands show. The upper band is populated with the non-ISL estimations, the second band with the GPS ISL system estimates and the third band with the LRI and KBR system estimates. When the GPS-like system facilitates the ISL, the accuracy of the estimation is about two times better, which is in line with the improved DOP, like mentioned in Subsection 2.1.2. It is also visible that the use of only one clock for the GPS ISL slightly increases the estimation accuracy with an average of about 2×10^{-5} m or 20 μm, because less parameters are estimated.

In the lower band, the estimation errors of the LRI and KBR, which are very similar, are visible. The results of the estimations with these systems are on average about four times better compared to the non-ISL solutions. This is due to the improved DOP values, like for the GPS ISL results, but because of the much smaller measurement noise that LRI and KBR contain, these results are two times smaller than those. The difference between estimating only one clock for the LPS constellation compared to nine clocks is 1×10^{-10} and 6×10^{-9} m for LRI and KBR, respectively, and therefore negligible.

The difference between LRI and KBR is minimal, only 1×10^{-7} m, but the LRI gives slightly better results, this is due to the lower noise and also because of the additional bias parameters that have to be estimated to make use of the KBR measurements.

In other words, considering only measurement noise, ISL gives substantial improvements to the estimation results. The ISL based on laser measurements is the best performing configuration, regardless of the capability to have the nine clocks in phase. In contrast, if GPS ISL is used, the accuracy can be improved by 20 μm when the clocks are in phase, and only one clock has to be estimated. The errors obtained are clearly random, and the results are spread over a spectrum of approximately 0 to 2 mm.

5.3. Ephemeris Error-only Simulation

Figure 10 shows the following simulation case to examine. This case includes noiseless observations, but introduces an error in the ephemeris like described in Subsection 4.6.

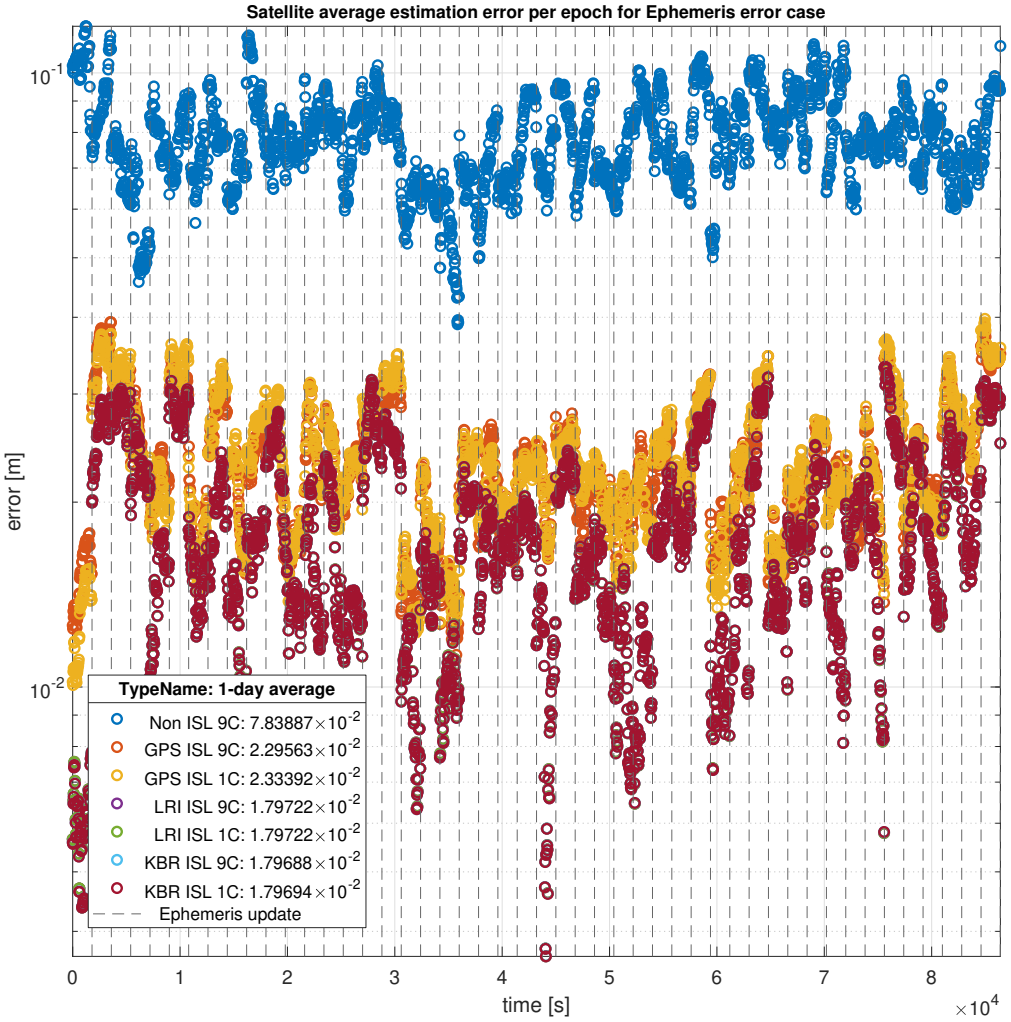

Figure 10: Satellite average of the LPS 3D position error over time when only ephemeris errors are included

The magnitude of the average errors for all system configurations is much higher than the ones obtained for the noise-only case. All the average position errors are in cm levels, while for the noise-only case, the errors were of sub-millimetres level. This difference suggests that the ephemeris error has a more substantial impact on the final position estimation.

Again, it is visible that the systems that do include ISL in the observations have a significant improvement in the solution as the GNSS only estimation

results are placed on some distance from the other results in the graph.

When GPS ISL is considered, the average estimation of the LPS satellite positions is about three times more accurate than GNSS only and when LRI or KBR measurements are used the accuracy of the solution improves even more than four times. The estimations provided by using the LRI and KBR systems once again are similar and have the highest accuracy, although the difference with GPS ISL is much smaller than in the noise-only case.

Inspecting the differences in the solution of estimating only one clock compared to estimating nine separate clocks, different outcomes are found as compared to the noise-only case. The accuracy of the estimation decreases when only one clock is estimated in the case of GPS ISL and KBR. This decrease is due to the systematic character of the ephemeris error, which can be absorbed when many parameters are estimated. The unknown, but systematic error is spread out over the different parameters to be estimated, so when there are more parameters, such as more clocks per epoch, the position error is smaller. The absorption is also the expected reason for the slightly better performance of the KBR system, for which the additional bias parameters have to be determined.

For GPS ISL, the nine clock configuration is about 0.4 mm more accurate, while for KBR the difference is only 0.6 μm, presumably because the biases already absorb a large part of the error. For the LRI system, the difference is about $1{\times}10^{-11}$ m and thus negligible, though still present.

Regarding systematic errors such as a GNSS ephemeris error, using ISL measurements is clearly beneficial. Using ISL improves the average error with 55 mm and even 5 mm more by using laser or K-band measurements. KBR is 3.5 μm more accurate than LRI, providing the most accurate results.

5.4. Noise and Ephemeris Error Simulation

The last simulation case is a semi-complete model, which includes both measurement noise and ephemeris errors. Figure 11 shows the estimation results, which are not much different from the ephemeris error-only simulation case. This absence of significant difference again stresses the fact that the ephemeris error is the dominant factor in the estimation. The accuracy of the estimations decreases, since the noise error is added, but only a few μm per configuration. The improvements of using ISL and the difference between GPS ISL, LRI and KBR are roughly equal to those values for the ephemeris error only case. So, using any form of LPS-to-LPS links results in

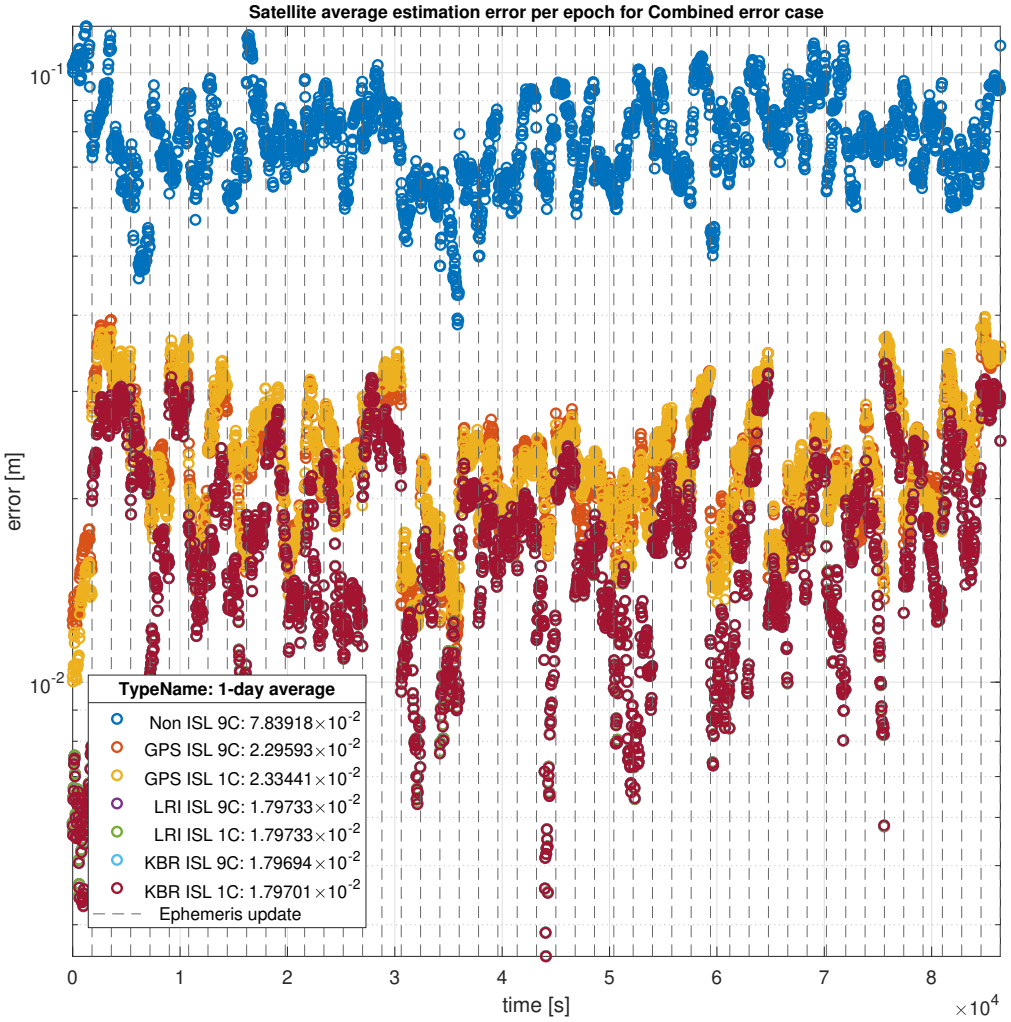

Figure 11: Satellite average of the LPS 3D position error over time when both errors are included

much higher accuracies for the estimation solution. The KBR system that estimates nine separate clocks provides the most accurate position estimates.

5.5. Complete Overview

Table 3 shows the average accuracies for the selected error cases and system configurations. The results are colour coded per column to show the performance of the system configurations per error case. In a column red cells denote the biggest errors and green the lowest errors, yellow and orange

cells denote intermediate results. The red colour of all the top cells indicate the non-ISL system, with the biggest positioning errors.

	None [m]	Noise [m]	Ephemeris [m]	Both [m]
Non ISL	2.86870×10^{-9}	9.65051×10^{-4}	7.83887×10^{-2}	7.83918×10^{-2}
GPS ISL	1.24456×10^{-9}	4.99859×10^{-4}	2.29563×10^{-2}	2.29593×10^{-2}
GPS ISL (1C)	9.86776×10^{-10}	4.80374×10^{-4}	2.33392×10^{-2}	2.33441×10^{-2}
LRI ISL	2.45143×10^{-9}	2.56643×10^{-4}	1.79722×10^{-2}	1.79733×10^{-2}
LRI ISL (1C)	2.47583×10^{-9}	2.56644×10^{-4}	1.79722×10^{-2}	1.79733×10^{-2}
KBR ISL	2.50189×10^{-9}	2.57408×10^{-4}	1.79688×10^{-2}	1.79694×10^{-2}
KBR ISL (1C)	2.49710×10^{-9}	2.57471×10^{-4}	1.79694×10^{-2}	1.79701×10^{-2}

Table 3: The 3D position error averaged over time and over all satellites for the four error cases and the seven system configurations, the colours show the relative system performance per column, green indicates the best and red the worst

6. Discussion

This section focuses on the insights that can be gained from the results in the previous section. Section 2 already gave a first indication of the valuable contribution that the inclusion of ISL can have on the lunar navigation system. The technique provides significant advantages for position estimation regarding the geometrical distribution.

After performing the estimation of the LPS satellites' position, better insight is obtained into the effect of the inclusion of different types of system configurations. In the previous section, the results are shared, and an initial perception is given. Here the results are examined in more detail, and the implications are discussed.

The most important thing to realise is that for all error cases, the estimation solution enhances significantly by introducing the observations between the LPS satellites self, regardless of the system configuration. Either using a system where the ISL consists of GNSS-like observations with code range and carrier phase measurements, using an optical measurement system like laser ranging, or employing K-band microwave observations, the average 3D position error decreases substantially.

6.1. Error Source Comparison

Regarding the error sources, it becomes evident that the ephemeris error, which is a systematic error, is the dominant error source. Comparing

the error cases of noise-only and ephemeris error-only, it is visible that the ephemeris error has a much larger impact on the estimation error. Also, when both error sources are included, the average errors vary minimally from the ephemeris error-only case, meaning that the ephemeris error is the driving source. This is in line with the expectations, as the ephemeris error is one of the most significant error sources in most GPS applications. Besides that, the error induced by the incorrect ephemeris is bigger than the measurement noise error. This difference in impact is interesting to keep in mind when a more complete simulation model is included for the estimations, and more systematic and random error sources are added. The sensitivity of different types of error sources and their magnitude is interesting for future research.

Continuing the comparison of the two distinct error sources, it becomes clear that the improvement in estimation accuracy achieved by the introduction of ISL is more prominent in the ephemeris error-only case. The error in the noise-only case decreases to 50% or even 26% of the error of the non-ISL system, depending on the ISL system configuration, while in the ephemeris case the error reduces to 30% or 22%. The error introduced in the latter case is significantly bigger, so there is more room for improvement in the accuracy by including ISL. However, the results also suggest that ISL proves to be very efficient in correcting for a systematic error. An explanation could be that the same incorrect GNSS positions are used by all the LPS satellites and that the linking of the satellites makes it easier to cope with the errors. This is an effect somewhat comparable to differential GPS.

6.2. System Configuration Comparison

From the comparison of the different system configurations, the following insights are obtained. Overall, a system that relies on optical or microwave range measurements achieves smaller estimation errors than a system with a GNSS-like observation system. An exception is the error-free simulation, but the estimation results, in this case, are almost entirely based on the computer rounding error, so they do not give much insight in the different systems.

The noise-only case shows that the system with the lowest noise level provides the most accurate position estimations as one would expect. Both LRI and KBR consist of measurements which are of much higher precision with a standard deviation of 0.1 and 30 μm, respectively, compared to the 1 m and 1 mm values for the code range and carrier phase measurements. LRI provides slightly better estimations because the measurements are more precise, but also unambiguous. The difference between the two is only about

1 μm (0.3%), while the noise level is 300 times lower for LRI. The noise of the GPS ISL phase measurement is 10^4 times bigger than the LRI noise, but the estimation error of GPS ISL is only two times bigger than the LRI error. KBR and GPS ISL have to estimate the same number of biases, so the difference in performance is mainly due to the measurement precision and number of measurements.

For the ephemeris error case, no noise is simulated, meaning that the precision of the measurements of the different systems is equal. The weights used for the various observations, however, are still equal to the inverse variance of the noise levels corresponding to the measurement types. Hence, this case uses the same weights as the associated noise case.

As the measurements are of equal precision, it would be expected that the system that provides the most measurements would perform the best. This would be GPS ISL as it provides both code and phase measurements, however, this is not the case. An argument would be that the GPS ISL requires the additional ambiguity estimations, which reduces the accuracy of the estimation solution. Nevertheless, here it should be noted the KBR ISL system also makes use of ambiguous measurements, and since the only difference is the type of measurements, the same amount of biases are estimated for both systems.

The findings of the previous section (cf. Table 3) show that the KBR system provides the most accurate estimation results. Therefore the number of extra bias parameters can not be the primary deteriorating influence on the estimation. The results show that the chosen observation weight is of extreme importance in the estimation of the satellite positions as this is the remaining factor that differentiates the systems at this point. The results show that the geometric advantages of the ISL incorporation can give a significant boost to the precision of the position determination, especially when the weights of the ISL observations are given the proper weighting.

The GPS ISL system has the lowest weights and provides the least accurate estimations. In contrast, the LRI system has the highest weight, but does not provide the most accurate estimation. This illustrates that merely selecting the highest weight does not work and that finding the proper weighting is an essential aspect of the estimation problem.

Interesting to notice is that the weight of LRI and KBR is 1×10^{14} and 1.1×10^{9}, respectively, a vast difference in the order of magnitude of 10^5, while the difference in estimation error is minimal. This also shows the sensitivity

to the weight and stresses the relevance of determining the correct weights.

The weights of all the distinct observations vary from each other, but the differences in the accuracy enhancement, compared with the non-ISL system, are relatively small, and the results of the ISL systems are more comparable.

The simulation using both the error sources confirms these insights. As the ephemeris error is the dominant source of errors, the magnitude of the different noise levels play a smaller role in the complete error model, and the results are very similar to the ephemeris error-only results. The weights are now more suitable for the noise levels, but the same conclusions can be drawn. KBR produces the most accurate position estimates, followed by LRI and GPS ISL after that. The relative improvements of the ISL systems with respect to the non-ISL configuration are also the same as in the ephemeris error-only case.

The increase in the position error of the complete error simulation compared to the noise-only simulation is slightly larger for LRI than for KBR. This difference suggests that ambiguous measurements are more resistant to systematic errors. A reason for this might be the absorption of the error in the extra parameters to be estimated. The increase in the position error for the two error cases is the smallest for GPS ISL. This system also makes use of ambiguous measurements. Moreover, this system contains more observations, which shows to be efficient against systematic errors.

6.3. Clocks in Phase Comparison

The last important aspect to consider is the ability of the system to have the satellite clocks in phase, requiring the estimation of only one clock for the entire system. In theory, as stated before, the solution should improve since fewer parameters are required to be estimated. For the GPS ISL system, this behaviour is indeed visible for the noise error-only case, where a small improvement in the estimation is visible. When the laser or microwave systems are considered, however, no significant change is visible. The ephemeris error case shows that the estimation results actually deteriorate when only one clock is estimated per epoch. This is because a systematic error, such as the ephemeris error, can be absorbed by the parameters to be estimated. By estimating multiple clocks, the systematic error can be spread over these parameters and appears in a smaller magnitude in the position estimates, for example. This is the case for GPS and KBR ISL, but for LRI, no real changes are seen, and the difference is negligible. The complete simulation

case shows the same outcome since the ephemeris error is the dominant factor.

Combining the results of this study, it can be stated that the KBR ISL system without including synchronised clocks can provide the best position estimations. This system achieves an average accuracy of 1.80 cm in absolute 3-dimensional position. Nonetheless, the results imply that the weights of the observations play a substantial role in the estimation accuracy. Therefore a future study should concentrate on finding optimal observations weight. The results, however, also suggest that the optimum of the accuracy lies close to 1.80 cm on average for the proposed compositions.

6.4. Alternative System Configuration Comparison

The achieved accuracies of the proposed systems are similar and lie around 1.80 cm; therefore, it is advisable to expand the comparison to other aspects of the systems. A cost-benefit analysis could be performed assessing the complexity, resources required, financial costs, weight and size to obtain a better comparison between the measurement types. A trade-off like that, is beyond the scope of this study, but here some fundamental aspects are discussed.

While the GPS ISL is the least performing, it uses a measurement type that is being used in navigation systems all the time. Therefore the system is flight-proven and has a low complexity to apply. Furthermore, GNSS observations use the same type of measurements, so the processing is expected to be more straightforward. In addition, this means that a GNSS receiver is located at the Earth pointing side of the satellite. With the assumptions for the receiver made before, this means that the satellites will be able to receive measurements from all directions. This way, it is also possible to include additional GNSS measurements in the estimation.

Both the LRI and KBR systems have been used for ISL before, but only between two satellites flying relatively close to each other in the GRACE and GRACE Follow On missions. Applying the measurement types for the large distances between the LPS satellites would be more challenging. The expectation is that the costs for these kinds of systems are much higher in comparison with the GPS ISL system. Also, the complexity of these systems is expected to be much higher, especially for the LRI as it uses directed lasers, which require some level of pointing accuracy and efficiently placed reflectors to link with LPS satellites in various directions. An advantage of the LRI system is that the optical ranging measurements are not affected by

the ionosphere, but since the LPS is designed to avoid the influence of the ionosphere as much as possible this is a minor advantage.

[30] proposes K-band ranging for ISL in PECMEO, which suggests the feasibility of the system. It is important to realise, however, that in the referenced work the envisioned application is to form a VLBI based space telescope, a type of missions usually much bigger and more expensive than navigation satellites.

6.5. Alternative Navigation Methods Comparison

Regardless of the choice of ISL system for LPS, the average attainable position accuracy of the LPS satellites is about 2 cm. With this ephemeris uncertainty lunar navigation of roughly 30 m can be provided when kinematic orbit determination is used, according to [24]. The subsequent discussion comparing LPS with state-of-the-art methods assumes these accuracy levels as the actual sensitivity of the lunar navigation precision with respect to the LPS ephemeris accuracy is still unknown and an interesting subject for further study.

Traditionally, navigation of lunar missions is carried out by ground tracking, requiring numerous ground station around the world tracking the satellite to determine its position accurately. Only a limited number of satellites can be tracked simultaneously by these ground stations, which means that remarkable improvements in infrastructure would be required to keep up with the increasing number of lunar missions. Ground tracking also focuses on a particular satellite instead of being able to follow all passing satellites.

Nonetheless, NASA's Deep Space Network (DSN) is expected to be able to achieve a position accuracy of 20 m in lunar orbit if a weighted batch least-squares method is used according to [43]. However, LADEE, which makes use of DSN, had the modest requirement of 4.3 km 3D position uncertainty and achieved 1.9 km in the worst-case scenario [44]. Comparable position errors are found for the Apollo 10 mission, which were higher than 1 km and even exceeded 10 km at times. Though, these values are expected to be similar to the real-time tracking capabilities of the future Orion mission, which makes use of DSN as well [45]. The SELENE mission also made use of ground tracking for navigation and achieved a position error around 50 m, but by using a combination of relay satellites and altimetry, the accuracy could be improved to approximately 20 m [46]. The Chang'E-2 ([47]) and Chang'E-3 ([48]) missions obtained accuracies between 30 and 45 m and between 20 and 30 m, respectively, by combining numerous ground stations to form VLBI

systems. The first is a surface imaging mission, and the latter consisted of a lander/rover combination, both requiring a significant level of position accuracy. There also exist terrain relative navigation techniques, which have the drawback of requiring a complete additional subsystem. These techniques can consist of altimetry leading to position accuracies in the order of 10 m, but they involve rather complex evaluations [49]. Another option is using an optical imaging system, which can provide the same order of accuracy, but only for low altitudes, while an accuracy of approximately 230 m is achieved at higher altitudes [50]. The disadvantage of the latter is that such techniques can only be used on the day-side of the Moon with appropriate illumination conditions.

Considering the achieved accuracies, requirements and predictions of some iconic missions, it is safe to say that the LPS with the expected accuracy, based on KOD, of roughly 30 m can come along with the other types of lunar navigation as the levels of precision are in the same order of magnitude. However, because of the one-way ranging GNSS technique, no complex additional systems are required, and less limitations in the form of altitude or lighting conditions are present. In addition, the LPS concept is future-proof as it supports any number of additional new Moon missions as long as they are equipped with the proper receiver.

Besides that, the prospected accuracy of LPS is in any case suitable for providing navigation solutions for missions similar to Apollo 10, the future Orion mission and LADEE-like missions.

As this study limits itself to the assessment of the position error of the LPS satellites themselves and not the precision of lunar navigation, a more thorough analysis on the latter would be required to conclude the feasibility of the proposed navigation system.

7. Conclusions

The presented study concentrated on investigating the accuracy of the position determination of LPS satellites in Polar-Equatorial Circular Medium Earth Orbits. The precise positioning of the LPS satellites is essential to reduce the ephemeris error of the constellation, which is shown to be of significant influence on the accuracy of lunar navigation facilitated by LPS. This study put great emphasis on the assessment of the incorporation of inter-satellite links in the navigation solution to enhance the position determination accuracy. This work focused for a large part on the mathematical

implications of the ISL measurement incorporation and the development of the expanded estimation tools. This section presents the conclusions that are drawn from the research performed and the discussion given before.

7.1. Error Sources

Section 4 explains the problem environment and observation simulation. As this work is the first study in this area, only the first steps in the simulation are set, and many error sources and force models are neglected at this stage. It was chosen to consider only measurement noise errors and GNSS ephemeris errors in this study because they are significant errors and have very distinct behaviour. The former error is a random source, while the latter is a systematic error source. By comparing the two, this work assesses the response of the positioning systems on the different sources. With these errors in place, sufficient insight can be gained in the performance of the system for this initial stage.

However, to get a more realistic representation of the performance, the way the errors are applied should be worked out in more detail. First of all, in this study, it is assumed that the noise level for a measurement type is normally distributed with a specific standard deviation, while in reality, the noise levels depends on numerous parameters. Besides that, this study shows that not the full range of noise levels could be included because of the limitations posed by the computer precision.

Secondly, the assumptions done around the simulation of the ephemeris can also be improved. The error is induced in the SMA only, while in reality the error may appear in additional orbital elements. Moreover, the refresh rate of 30 minutes should also be reconsidered as ephemeris updates occur less frequent in reality. The obtained results are thus based on an optimistic GNSS ephemeris assumption.

In addition to reevaluating the errors used in this study, an overview of additional error sources and their behaviour and magnitude has to be created to obtain a more complete view on the performance of the proposed navigation system.

Creating this overview and listing all different error sources is beyond the scope of this study and could be the subject of entire new paper. It is recommended, however, to investigate the effect of satellite clock errors and ionospheric delay. These are two error sources that can also cause significant errors in many GPS applications [23].

The inclusion of the LTC is another way to improve the realism of the results obtained with the developed tools. As the tool to simulate the measurements is already in place, an extension of this research might be the LTC integration in the kinematic estimation approach for the ISL.

These are just a few examples of subjects for future research aiming to enhance the current model. The simulation environment used in the presented work, however, is sufficient to achieve the goal of this study, which is to show the effect of including ISL to the navigation problem and comparing different methods of ISL.

7.2. System Configurations

These different methods combined with the various error sources form the assessment cases discussed in Section 3. Different forms of the system under various circumstances are tested and compared with a non-ISL configuration to gain a good insight in the effects of the inclusion of ISL and its potential. This work identifies seven different system configurations that differ significantly regarding measurement precision, measurement type and measurement instrument. The study shows that the accuracy of the position estimation of the LPS satellite increases significantly by including ISL observations as the errors of the estimation decrease at least by a factor 3.3 when both error sources are considered. This is a vast improvement, but the actual improvements depend on the system used. First thing to indicate, is that the test results of this study suggest that the ability of the system to have the satellite clocks in phase is not interesting as the estimation accuracy declines rather than it improves. It should be mentioned, however, that the clock synchronisation might have advantages when actual clock errors are simulated. This gives another reason for future studies to investigate that particular error source.

The differences in accuracy between the three distinct ISL systems are not very big, especially not between the LRI and KBR systems which have almost identical positions errors. The achieved accuracy in the average absolute position error of the LPS satellites is 2.30 cm and 1.80 cm for the GPS ISL and the LRI or KBR systems, respectively. Since the accuracy results of the proposed system configurations are similar, the comparison of other aspects could offer ways to select the most appropriate system. Section 6 already suggests that a cost-benefit analysis could provide a better judgement for the attractiveness of the proposed systems. Cost, in this context, is not only monetary, but also, for example, size, weight and complexity related.

In reality, more elements to consider for the trade-off between the methods of ISL exist, but these aspects offer a good beginning. While the GPS ISL system is the least performing configuration in this study, the configuration should not be disregarded as it may outperform the other system on other aspects, like cost or complexity. Besides the system to system comparison, this inquiry also grants an indication of the overall resources required for LPS. Later design phases require this indication to make a trade-off between the envisioned lunar navigation improvement and investment. For such a study, it is also essential to establish constraints on the weight and cost of the instrument posed by the mission requirements.

7.3. LPS Feasibility

According to the LPS study mentioned earlier, an ephemeris error of 1.78 cm in the absolute position at the end of an ephemeris arc leads to a viable navigation system for lunar spacecraft [24]. The presented work showed that the average absolute position error is roughly 2 cm for any of the systems, which is higher, even though it differs only 10% from the value in the past study. This leads to the question if the use of ISL can provide LPS ephemerides that are accurate enough for lunar navigation. After all, the current study includes not all error sources in the simulations yet, and besides that, it assumes an optimistic GNSS ephemeris error, while this is the dominant error source. Therefore, the position determination accuracy of the LPS satellites and thus the LPS ephemerides could turn out less precise. On the other hand, there are many aspects that improve the accuracy of the positioning, which are not yet or not completely considered in this research. The accuracy already achieved and the number of these aspects justify the further research of the aspects to determine the full capabilities of LPS. First of all, the orbital arrangement of the LPS constellation is not optimised. As mentioned earlier, the PECMEO concept is expected to offer many advantages. An optimisation of certain orbital elements, like the altitude, the longitude of the ascending node and the argument of periapsis, however, could offer even more advantages. Such an optimisation should focus on the DOP values achievable, aiming for an average low DOP value, but also a constant DOP over time. It is important to realise that the constellation has to be optimised for its own LPS positioning, but also with respect to the lunar navigation performance. The former is expected to drive the altitude down, while the latter improves with a higher altitude. Besides that, avoiding atmospheric influences, like ionospheric delay and remaining outside

the Van Allen belts pose additional constraints to the orbital design. During the presented study, a tool calculating the DOP values of the satellites is already developed. The tool could be a good starting point for a future study focusing on the optimisation of the orbital arrangement of the constellation.

Also, as is discussed in Section 6, the weights given to the observations in the estimation have a considerable influence on the accuracy outcome. Although the results suggest that limits in accuracy exist for the current composition, determining alternative observation weights could enhance the navigating solution. Variable weighting for separate observations and weight optimisation is an interesting subject for future work.

Besides that, an improved estimation can also be achieved by making use of additional estimation algorithms. The position determination methods used in the current study do not consider the satellite motion in their models. By expanding the position determination tools suitable for ISL with dynamical approaches, it is expected that higher accuracies will be achieved. The modifications applied in this study could be used as a starting point for a follow-up study focusing on developing additional navigation tools for ISL applications. In a study like this, the environment has to be more detailed, and the simulations have to be done using a higher fidelity force model. This is because, for example, dynamic or reduced-dynamic orbit determination methods make use of accelerations exerted by the environment.

Furthermore, the inclusion of additional transmitters in the system can improve the geometry and hence the estimation accuracy, comparable to the inclusion of the ISL. In reality, there are more navigation systems available around the Earth that can help enhance the position accuracy of the LPS constellation by providing additional observations and an improvement in geometry. Extra observations can also originate from the ground if measurements received from ground stations on Earth are used for the LPS positioning. Whereas the first option also involves additional transmitter ephemeris errors, in the second option the transmitter position is known with extremely high accuracy. The use of ground station measurements, however, goes against the intention of being autonomous and independent of ground interference.

This section gives many suggestions on how the precision of the LPS position estimation can be improved, and hence, how the LPS ephemeris error can be reduced. This reduction in ephemeris error might be required to provide a viable navigation system for lunar travel. A significant contribution to the current work would be a sensitivity analysis of the LPS ephemeris error

with respect to the lunar navigation accuracy. This way, the required LPS position precision to achieve desirable navigation accuracy levels for lunar applications can be established. Besides, the acceptable or even necessary increases in system complexity to achieve this can be determined. Such a study could provide a trade-off in the complexity of the LPS system and the provided lunar navigation accuracy.

The results found in this study suggest that the LPS concept is a feasible navigation system for specific lunar applications such as, for example, Apollo-like spacecraft en route for the Moon. The results of this work also point towards the added value of LPS for new lunar applications. Although this can not be confirmed yet, further study to investigate this is warranted. Even though the shown accuracy and the anticipated improvements suggest that LPS can provide means of navigation comparable to the current state-of-the-art and probably even better, while being less demanding and more flexible, a thorough assessment of expected navigation requirements is recommended. A study mapping future lunar missions and their requirements can give better insight regarding the advantages of the LPS and its feasibility.

Taking all the considerations, limitations and prospects of the current study into account, it can be concluded that it is interesting to further explore the LPS concept. The estimated LPS position accuracy achieved in this study is approximately on the level of being acceptable for lunar navigation. Besides, expectantly there is enough room to further improve this accuracy to ensure that sufficient accurate ephemerides will be provided. Some additional studies might be required to establish the feasibility conclusively. Besides that, this study shows that the proposed LPS concept has considerable advantages over current and past navigation systems, which stresses the value of further investigation of the subject.

Additionally, besides the suitability for the envisioned application of lunar navigation, this study shows the tremendous advantages of inter-satellite linking for satellite orbit determination and navigation problems. These advantages give sufficient reason to further explore the possibilities of ISL and the development of estimation algorithms suitable for multi-satellite problems. The presented study forms a great starting point for future studies and the tools developed for this research can be used in all subsequent applications that desire to incorporate inter-satellite linking.

References

[1] LSPET*, Preliminary examination of lunar samples from apollo 11, Science 165 (3899) (1969) 1211–1227, *Lunar Sample Preliminary Examination Team.
URL http://www.jstor.org/stable/1727968

[2] T. Gill, Nasa's lunar orbital platform-gateway, in: The Space Congress Proceedings 2018 (45th): The Next Great Steps, 2018, pp. 4–17.

[3] J. O. Burns, B. Mellinkoff, M. Spydell, T. Fong, D. A. Kring, W. D. Pratt, T. Cichan, C. M. Edwards, Science on the lunar surface facilitated by low latency telerobotics from a lunar orbital platform-gateway, Acta Astronautica 154 (2019) 195–203.

[4] S. Fukuda, S.-i. Sakai, E. Sato, S. Sawai, S. WG, SLIM: Small explorer for technology demonstration of lunar pinpoint landing, in: The 24th Workshop on JAXA Astrodynamics and Flight Mechanics, 2014, p. 109.

[5] D.-Y. Rew, G. Ju, S. Lee, K. Kim, S.-W. Kang, S.-R. Lee, Control system design of the korean lunar lander demonstrator, Acta Astronautica 94 (1) (2014) 328–337.

[6] J. N. Goswami, M. Annadurai, Chandrayaan-2 mission, in: Lunar and Planetary Science Conference, Vol. 42, 2011, p. 2042.

[7] Q. Wang, J. Liu, A chang'e-4 mission concept and vision of future chinese lunar exploration activities, Acta astronautica 127 (2016) 678–683.

[8] P. D. Spudis, The moon: Port of entry to cislunar space, Toward a Theory of Space Power: Selected Essays.

[9] T. M. Perrin, J. G. Casler, Architecture study for a fuel depot supplied from lunar resources, in: AIAA SPACE 2016, Aerospace Research Central, 2016, p. 5306.

[10] F. Tronchetti, The moon agreement in the 21st century: Addressing its potential role in the era of commercial exploitation of the natural resources of the moon and other celestial bodies, J. Space L. 36 (2010) 489.

[11] M. T. Zuber, D. E. Smith, M. M. Watkins, S. W. Asmar, A. S. Konopliv, F. G. Lemoine, H. J. Melosh, G. A. Neumann, R. J. Phillips, S. C. Solomon, et al., Gravity field of the Moon from the Gravity Recovery and Interior Laboratory (GRAIL) mission, Science 339 (6120) (2013) 668–671.

[12] C. Hardgrove, J. Bell, J. Thangavelautham, A. Klesh, R. Starr, T. Colaprete, M. Robinson, D. Drake, E. Johnson, J. Christian, et al., The Lunar Polar Hydrogen Mapper (LunaH-Map) mission: Mapping hydrogen distributions in permanently shadowed regions of the Moon's south pole, in: Annual Meeting of the Lunar Exploration Analysis Group, Vol. 1863, 2015, p. 2035.

[13] I. Karachevtseva, A. Kokhanov, A. Konopikhin, I. Nadezhdina, A. Zubarev, V. Patratiy, N. Kozlova, D. Uchaev, D. V. Uchaev, V. Malinnikov, et al., Cartographic and geodetic methods to characterize the potential landing sites for the future russian missions luna-glob and luna-resurs, Solar System Research 49 (2) (2015) 92–109.

[14] F. Li, M. Ye, J. Yan, W. Hao, J.-P. Barriot, A simulation of the four-way lunar lander–orbiter tracking mode for the chang'e-5 mission, Advances in Space Research 57 (11) (2016) 2376–2384.

[15] L. Alkalai, B. Solish, J. Elliott, T. McElrath, J. Mueller, J. Parker, Orion/MoonRise: A proposed human & robotic sample return mission from the Lunar South Pole-Aitken Basin, in: 2013 IEEE Aerospace Conference, IEEE, 2013, pp. 1–10.

[16] E. S. Steenstra, D. J. Martin, F. E. McDonald, S. Paisarnsombat, C. Venturino, S. O'Hara, A. Calzada-Diaz, S. Bottoms, M. K. Leader, K. K. Klaus, et al., Analyses of robotic traverses and sample sites in the Schrödinger basin for the HERACLES human-assisted sample return mission concept, Advances in Space Research 58 (6) (2016) 1050–1065.

[17] L. Bucci, A. Colagrossi, M. Lavagna, Rendezvous in lunar near rectilinear halo orbits, Advances in Astronautics Science and Technology 1 (1) (2018) 39–43.

[18] L. Qiao, Z. Ling, X. Fu, B. Li, Geological characterization of the chang'e-4 landing area on the lunar farside, Icarus 333 (2019) 37–51.

[19] M. Djachkova, M. Litvak, I. Mitrofanov, A. Sanin, Selection of luna-25 landing sites in the south polar region of the moon, Solar System Research 51 (3) (2017) 185–195.

[20] M. Martin-Neira, V. Kudriashov, I. Barat, B. Duesmann, E. Daganzo, PECMEO: a New Space-to-Space Connected-Element VLBI Concept, In Proceedings of the ARSI'17 Workshop (2017) 6.

[21] J. A. Christian, E. G. Lightsey, Review of options for autonomous cislunar navigation, Journal of Spacecraft and Rockets 46 (5) (2009) 1023–1036.

[22] G. N. Holt, B. A. Wood, Sextant navigation on the international space station: A human space exploration demo, in: 42nd Annual AAS Guidance, Navigation and Control Conference, NASA Johnson Space Center, 2019, pp. 1–15.

[23] E. Kaplan, C. Hegarty, Understanding GPS: principles and applications, 2nd Edition, Artech house, 2006.

[24] M. A. Griffioen, Assessment of Lunar Positioning Accuracy with PECMEO Navigation Satellites, type, TU Delft, Kluyverweg 1, Delft, note (2020).

[25] E. Davis, C. Dunn, R. Stanton, J. Thomas, The GRACE mission: meeting the technical challenges, American Institute of Aeronautics and Astronautics, 1999.

[26] J. J. Spilker Jr, P. Axelrad, B. W. Parkinson, P. Enge, Global Positioning System: Theory and Applications, Volume I, American Institute of Aeronautics and Astronautics, 1996.

[27] Kroes, R., Precise Relative Positioning of Formation Flying Spacecraft using GPS, Ph.D. thesis, Delft University of Technology (Apr. 2006). URL http://resolver.tudelft.nl/uuid:1a68ee94-3d55-44b9-9d8b-25fa44e96922

[28] D. Dirkx, E. Mooij, B. Root, Propagation and estimation of the dynamical behaviour of gravitationally interacting rigid bodies, Astrophysics and Space Science 364 (2) (2019) 37.

[29] M. MARTIN-NEIRA, V. KUDRIASHOV, I. BARAT, B. DUESMANN, E. DAGANZO, Space-to-space Radio Interferometry System from Medium Earth Orbits, Chin. J. Space Sci. 39 (4) (2019) 28.

[30] K. Volodymyr, M.-N. Manuel, B. Itziar, M. I. Pertonilo, D.-E. Elena, A. Nader, V. Vaclav, System Design for the Event Horizon Imaging Experiment Using the PECMEO Concept, Chin. J. Space Sci. 39 (2) (2019) 250–266. doi:10.11728/cjss2019.02.25.

[31] J. R. Yim, J. L. Crassidis, J. L. Junkins, Autonomous orbit navigation of two spacecraft system using relative line of sight vector measurements, in: Proceedings of the AAS Space Flight Mechanics Meeting, 2004, pp. 1–14.

[32] M. L. Psiaki, Autonomous orbit determination for two spacecraft from relative position measurements, Journal of Guidance, Control, and Dynamics 22 (2) (1999) 305–312.

[33] O. Brown, P. Eremenko, Fractionated space architectures: A vision for responsive space, Tech. rep., DEFENSE ADVANCED RESEARCH PROJECTS AGENCY ARLINGTON VA (2006).

[34] N. Herscovici, C. Christodoulou, V. Lappas, G. Prassinos, A. Baker, R. Magnuss, Wireless sensor motes for small satellite applications, IEEE Antennas and Propagation Magazine 48 (5) (2006) 175–179.

[35] R. Wolf, Satellite orbit and ephemeris determination using inter satellite links, Ph.D. thesis, Bundeswehr University Munich (2001).

[36] R. B. Langley, et al., Dilution of precision, GPS world 10 (5) (1999) 52–59.

[37] K. Abich, A. Abramovici, B. Amparan, A. Baatzsch, B. B. Okihiro, D. C. Barr, M. P. Bize, C. Bogan, C. Braxmaier, M. J. Burke, et al., In-orbit performance of the grace follow-on laser ranging interferometer, Physical review letters 123 (3) (2019) 031101.

[38] O. Montenbruck, Kinematic GPS positioning of LEO satellites using ionosphere-free single frequency measurements, Aerospace Science and Technology 7 (5) (2003) 396–405. doi:10.1016/S1270-9638(03)00034-8.

URL http://www.sciencedirect.com/science/article/pii/S1270963803000348

[39] J. G. Walker, Satellite constellations, Journal of the British Interplanetary Society 37 (1984) 559–572.

[40] U. S. DoD, Global positioning system standard positioning service performance standard 5th edition (2020).

[41] M. S. Braasch, A. Van Dierendonck, Gps receiver architectures and measurements, Proceedings of the IEEE 87 (1) (1999) 48–64.

[42] C. Dunn, W. Bertiger, Y. Bar-Sever, S. Desai, B. Haines, D. Kuang, G. Franklin, I. Harris, G. Kruizinga, T. Meehan, et al., Instrument of GRACE: GPS augments gravity measurements, GPS World 14 (2).

[43] M. Woodard, D. Cosgrove, P. Morinelli, J. Marchese, B. Owens, D. Folta, Orbit determination of spacecraft in earth-moon l1 and l2 libration point orbits, AAS/AIAA Astrodynamics Specialist Conference (AAS 11-514).

[44] A. Kam, L. Plice, K. F. Galal, A. M. Hawkins, L. A. Policastri, M. Loucks, J. P. Carrico, C. A. Nickel, R. L. Lebois, R. Sherman, Ladee flight dynamics: Overview of mission design and operations, in: Proceedings of the 25th AAS/AIAA Space Flight Mechanics Meeting, 2015, pp. 11–15.

[45] C. D'Souza, T. Crain, F. Clark, J. Getchius, Orion cislunar guidance and navigation, in: AIAA Guidance, Navigation and Control Conference and Exhibit, 2007, p. 6681.

[46] S. Goossens, K. Matsumoto, D. D. Rowlands, F. G. Lemoine, H. Noda, H. Araki, Orbit determination of the SELENE satellites using multi-satellite data types and evaluation of SELENE gravity field models, Journal of Geodesy 85 (8) (2011) 487–504. doi:10.1007/s00190-011-0446-2.

[47] P. Li, X. Hu, Y. Huang, G. Wang, D. Jiang, X. Zhang, J. Cao, N. Xin, Orbit determination for chang'e-2 lunar probe and evaluation of lunar gravity models, Science China Physics, Mechanics and Astronomy 55 (3) (2012) 514–522.

[48] Y. Huang, S. Chang, P. Li, X. Hu, G. Wang, Q. Liu, W. Zheng, M. Fan, Orbit determination of chang'e-3 and positioning of the lander and the rover, Chinese science bulletin 59 (29-30) (2014) 3858–3867.

[49] E. Mazarico, G. A. Neumann, M. K. Barker, S. Goossens, D. E. Smith, M. T. Zuber, Orbit determination of the lunar reconnaissance orbiter: status after seven years, Planetary and space science 162 (2018) 2–19.

[50] V. S. Bilodeau, S. Clerc, R. Drai, J. de Lafontaine, Optical navigation system for pin-point lunar landing, IFAC Proceedings Volumes 47 (3) (2014) 10535–10542.

3

Conclusions and Recommendations

In this thesis, the position determination accuracy of LPS satellites in a PECMEO constellation using different system configurations is assessed. The purpose of this is twofold: on the one hand, to obtain an indication of the achievable LPS ephemeris error and the feasibility of the lunar navigation concept, and on the other hand, to assess and compare different ISL techniques to demonstrate their influence and impact on orbit determination. This chapter evaluates the results of the work and answers the research questions in section 3.1. After that, section 3.2 will provide recommendations for future work.

3.1. Conclusions

To answer the research questions from section 1.1, the findings of the paper are used and presented here in the structure of the questions. This section provides the answers to the research questions and sub-questions separately.

1. ***What modifications of existing least-squares algorithms are required to make them suitable for navigation using ISL?***

   To create least-squares estimator algorithms that are suitable for orbit determination applications that make use of ISL, some significant alterations are required. The main difference with the existing algorithms is the requirement of the simultaneous estimation of the positions and clock offsets of the separate satellites. This is necessary because the ISL observations originate from the position of a transmitting LPS satellite which is being determined as well. Due to this requirement, the sizes of the design and normal matrices increase significantly, and it becomes essential to handle the entries cautiously. If this difference is honoured correctly, the traditional algorithms can be followed. A complete answer is provided by answering the following sub-questions.

   (a) *What are the differences between standard observations and ISL observations?*
   The standard observations originate from GNSS satellites and the ISL observations from other LPS satellites. While the positions of the former are broadcasted, the positions of the other LPS satellites are being estimated as well. In the estimation process, the pseudorange between receiver and transmitter is modelled based on these positions. Hence, in order to obtain an accurate estimation for both the receiver and transmitter, both their positions and clock offsets have to be estimated.

   (b) *What modifications are required in the SPP algorithms to make them suitable for ISL observations?*
   An LPS satellite is always able to communicate with at least one LPS satellite in another orbital plane and both LPS satellites in its own orbital plane. Therefore, the LPS satellites are all interconnected at any moment. Considering the difference between the observations and the handling of them described in the previous answer, this means that the positions and clock offsets of the nine LPS satellites have to be determined simultaneously at every epoch. Hence, the partial derivatives of every observation with respect to these 36 parameters have

to be determined. Therefore, the design matrix contains 36 columns, and the normal matrix is a 36-by-36 matrix, instead of the standard 4 columns and 4-by-4 matrix. The partial derivative of the transmitter parameters is equal but of opposite sign to the partial derivative of the receiver parameters for the ISL observations. The remainder of the algorithm stays unchanged.

(c) *What modifications are required in the KOD algorithms to make them suitable for ISL observations?*
The KOD and SPP algorithms share many similarities and the modifications for ISL suitability are comparable. The difference of the KOD scheme is that the epochs are interconnected by the bias measurements and thus that the batch least-squares method estimates the positions and clock offsets for all epochs simultaneously. For the ISL applications, this means that the parameters of all LPS satellites at every epoch are determined at once. Besides that, the bias parameters have to be estimated. In the complete normal matrix the upper left corner, corresponding to the position and clock offset partial derivatives, is a block diagonal matrix with 36-by-36 matrix blocks on the diagonal. In the original KOD algorithm, the blocks on the diagonal are 4-by-4 matrices. The blocks are modified along the lines of the adjustments described in the previous answer to accommodate for the 36 parameters. The upper right and bottom left corner, corresponding to the bias parameters, interconnect the position estimates over the epochs. These matrix elements contain much more entries than these partitioned matrices in the original algorithms. This is due to the incorporation of biases between transmitters and nine different satellites, and the interconnected ISL biases that relate to two satellites. Because of the described changes, the size of the matrices used in the estimation increases significantly. Hence, it becomes even more essential to use the sparsity of the normal matrix and intermediate inversion of the 36-by-36 sub-matrices on the diagonal to efficiently solve the normal equations to obtain estimated corrections.

(d) *What modifications are required in the LSQ algorithms to make them suitable for systems with synchronised clocks?*
The ability to have the clocks of the constellation in phase is only applied to the KOD algorithms for ISL applications. Therefore, it mainly adopts the alterations described in the answer to the previous question. When the clocks of the system are synchronised, only one clock offset has to be determined per epoch, instead of nine separate clocks offsets. This means that 28 parameters have to be determined per epoch. Following the changes described in the previous answer, the sub-matrices on the diagonal of the upper left corner of the normal matrix are now 28-by-28 matrices. The other difference with the KOD ISL algorithm is that for the ISL the clock offset error is zero, as the satellites have a synchronised clock. Other aspects of the scheme remain the same as for the KOD ISL scheme.

2. ***What improvement in the accuracy of the position estimation of the LPS satellites can be achieved using Inter-Satellite Linking?***

The answers on the sub-questions are based on the complete error model as this gives the most realistic results. That means that a model including measurement noise errors and GNSS ephemeris errors is used. It is shown in the presented study that an average position accuracy of 7.84 cm can be achieved when ISL is not considered. Including ISL observations leads to an average accuracy of 1.80 cm when KBR ISL measurements are used. This is an accuracy improvement of more than four times, which is a remarkable enhancement. The ISL technique for orbit determination shows to be a promising technique and warrants future research into the subject to be able to apply it in its full extent.

(a) *What position accuracy can be achieved for the LPS satellites using an SPP LSQ estimator without ISL observations?*
Using the SPP algorithm means that only the GNSS observations are used, which have a standard deviation of 1 m. Hence, the achievable accuracy is expected to be around 1 m, depending on the PDOP. The SPP algorithm yields a solution with an average 3D position accuracy of 1.34 m.

(b) *What position accuracy can be achieved for the LPS satellites using a KOD LSQ estimator without ISL observations?*

When the kinematic least-squares estimator is used, the carrier phase measurements received from the GNSS satellites can also be used. These measurements are much more precise and have a standard deviation of 1 mm. The KOD algorithm provides position estimates with an accuracy of 7.84 cm on average. This is a significant improvement compared to the SPP scheme. For ISL applications, only the KOD algorithm is considered.

(c) *What position accuracy can be achieved for the LPS satellites using a KOD LSQ estimator with ISL observations?*
The ISL measurements are included in the observations to answer this question. This means that the modified algorithms have to be used to process the observations correctly. For this step, different options can be considered regarding the type of measurements used, which are addressed in the next sub-question. The best result that is obtained with the KOD ISL algorithm is 1.80 cm, when the KBR system is used.

(d) *What is the impact on the position accuracy of using different measurement system configurations?*
As different measurement systems can be used for the ISL observations, it is important to determine the effects of the various proposed systems. This study considered a traditional GPS-like measurement system that provided 2.30 cm accuracy position estimates by deploying range measurement and phase measurements with a standard deviation of 1 m and 1 mm, respectively. LRI is another proposed system configuration that uses very precise range measurements with a standard deviation of 0.1 μm. This system produced position results with an accuracy of 1.80 cm on average. The third system configuration, KBR, using microwave phase measurements with a 30 μm standard deviation, provided 1.80 cm accuracy estimates as well. The KBR system resulted in the best accuracy, but only approximately 4 μm better than the LRI system. There is a clear difference between the results of the various systems. The number of observations or the number of parameters to be estimated do not seem to be of significant influence. The precision of the measurement system does have an impact, since the LRI and KBR systems perform significantly better than GPS ISL. However, the effect of the precision is limited as the KBR with less accurate measurements slightly outperforms the LRI system. Assigning appropriate weights to the observations in the estimation process shows to be a delicate task, that allegedly has a significant impact on the resulting accuracies.

(e) *What is the impact on the position accuracy of the synchronisation of the LPS satellite clocks?*
This study shows that applying the constellations' ability to have its satellites' clocks in phase is of minimal influence in the used set-up. Simulations comparing the synchronised systems with systems without their clocks in phase presented minimal differences. The results show that the accuracy of the position determination even reduces. This is only a reduction of about 4 μm for GPS ISL, 0.7 nm for KBR and an even smaller reduction for LRI.

(f) *What is the impact on the position accuracy of including random and systematic error sources to the model?*
As expected, including more error sources in the model leads to less accurate position estimates. The difference in accuracy between GNSS ephemeris errors only and both ephemeris and measurement noise errors, however, is minimal. This shows that the ephemeris error is the dominant error source in the considered model. Besides determining the most significant error source, the difference in impact between the system configuration is interesting to note. Comparing the error-free simulation results with the noise-only simulation results, LRI has the smallest increase in the estimation error. Its measurements have the lowest noise level as it is best resistant to measurement noise. When the complete error simulations are compared to the noise-only cases, a bigger increase in the position error is seen for LRI and KBR than for GPS ISL. This suggests that more measurements in the estimation reduces the impact of systematic errors. The increase in the position error for LRI is slightly bigger than the increase for KBR. This points towards the beneficial use of ambiguous measurements for systematic errors. The systematic error can be absorbed by the extra bias parameters that have to be estimated. Note that if only range measurements are used, the effects of systematic errors also could be reduced by estimating extra parameters.

3.2. Recommendations

Based on the results and conclusions of the presented research, various recommendations for future work is specified. These recommendations highlight the subjects of the study that warrant an extension of the research on the proposed lunar navigation system and the use of inter-satellite linking in orbit determination. After performing such an innovative study, countless recommendations for the future can be done. This work is one of the first studies in the area of lunar navigation provided by a PECMEO constellation, so three different directions are defined for future study subjects.

Firstly, it would be interesting to do more research on the LPS concept. An assessment of the possible system configurations for the ISL and a trade-off of the configurations would give a better insight in the achievable accuracy of the LPS position determination.

A sensitivity analysis of the lunar navigation accuracy with respect to the LPS ephemeris error provides a better understanding of the desired or even necessary LPS positioning accuracy. This way, a broader context will be offered to the current study. Besides that, an extra dimension can be added to the trade-off mentioned above. The determination of requirements for the lunar navigation system would be a great asset in such work. Studying alternatives for lunar navigation would provide more background here.

Another topic within this direction recommended to pursue is the investigation of the improvement of the estimation accuracy. It is advised to perform an optimisation of the orbital arrangement of the LPS constellation. The DOP tool built in this study offers a good starting point for such a study. Investigating the option of additional transmitters, such as other navigation constellations or ground stations, is another opportunity.

Another way to obtain improved accuracy estimations is to expand the estimation algorithms. This grants another direction of research derived from the presented study. This direction focuses more on the ISL technique. In this study, algorithms suited for ISL for point positioning and kinematic orbit determination are developed. A future study could take it a step further by writing ISL suitable algorithms for dynamic orbit determination. Such a study could begin with reduced dynamic estimators and later proceed to pure dynamic orbit determination. [7] clearly explains the reduced dynamic orbit determination method. The work of Kroes in combination with the ISL modification explanation presented in the current study offers a good starting point for this.

A third research direction recommended based on the presented work is the expansion of the simulation model. This study uses Kepler orbits for the satellite orbit simulation. Hence, it uses the gravitational force of the Earth as only acceleration. By implementing a high fidelity force model, a more realistic propagation of the satellites can be simulated. As a result, more astrophysical and technological aspects of a real navigation mission can be considered, such as the accuracy of the instruments and the effect of the environment on the instruments.

A study in this area could also focus on the simulation of a more complete error model. This thesis considered only GNSS ephemeris errors and measurement noise errors.

Studying additional error source could form a significant contribution to a realistic representation of the navigation capabilities. Satellite clock errors and ionospheric path delays are significant error sources in Earth navigation problems. Therefore, it is advised to include at least these error sources in such a study. Additionally, the light-time correction can be incorporated in the kinematic orbit determination algorithms to include the effect of the signal travel times between satellites.

Besides including additional error sources, the currently used error sources could be studied to a more significant extent, enabling a more realistic representation of them. Because of the assumptions made in this thesis, the full impact of the errors is not covered. Another advantage of a more detailed study of the used error sources is that it possibly provides more appropriate weights for the observations. The presented work showed that the weights of the observations play a substantial role in the estimation accuracy.

A

Verification and Validation

This appendix elaborates on the verification and validation of the major numerical techniques employed during this thesis.

The simulations and computations performed in this research heavily depend on the TU Delft Astrodynamics Toolbox (Tudat). Tudat contains many libraries that can be used for the simulation and orbit determination. The tools found in the built-in Tudat libraries are all already verified and validated. Hence, this work uses them as such. These tools include the simulation of the satellite orbits, the creation of the ephemerides and the simulation of measurement observations. The toolbox also contains the visibility checker that determines if an observation between two link ends is possible at a specific epoch.

This appendix focuses on the tools and algorithms built for this thesis work. The tools added to the existing body of knowledge mainly consist of the estimation algorithms written for this study. These are the Single Point Positioning (SPP) algorithm, the Kinematic Orbit Determination (KOD) algorithm, the Single Point Positioning for ISL (SPPISL) algorithm and the Kinematic Orbit Determination for ISL (KODISL) algorithm.

A.1. Error-free Simulation Verification

This work uses the algorithms to perform position estimations for simulated satellites. For this reason, it is easy to verify the methods since they should provide estimates close to the simulated positions. This is the primary method of verification of the algorithms; in the case that no errors are simulated for the observations, the error-free input for the estimation scheme should provide near-perfect estimations. The absolute 3-dimensional difference between the estimated positions and the true simulated positions per epoch is determined and averaged over the nine LPS satellites. This difference produces the estimation error, which should be approaching zero for error-free observations.

Figure A.1 shows the estimation error of the created algorithms for a 24-hour arc and the average estimation error per algorithm. The figure shows that the errors are in the order of magnitude of 10^{-9} m. This value is extremely close to zero and already suggests a correct functioning of the algorithms. The small deviation from zero is induced by the rounding error of the computer used. 64-bit computations are used in this study, providing a 15 to 16 digits precision for values. The absolute positions of the satellites are in the order of magnitude of 10^{7} m, as the orbital altitude is 14,000 km. That means that digits around 10^{-8} and 10^{-9} might be lost because of the precision limitations. This shows that the small errors in the estimations can be attributed to the rounding error of the computer. The results show that, aside from the rounding error, all estimators provide perfect position solutions and thereby verify the algorithms.

A.2. Point Positioning Verification

Many numerical examples exist for point positioning; these can be used as an extra validation for the SPP algorithm. In [10] such a numerical example is found at page 415. The SPP algorithm build for this

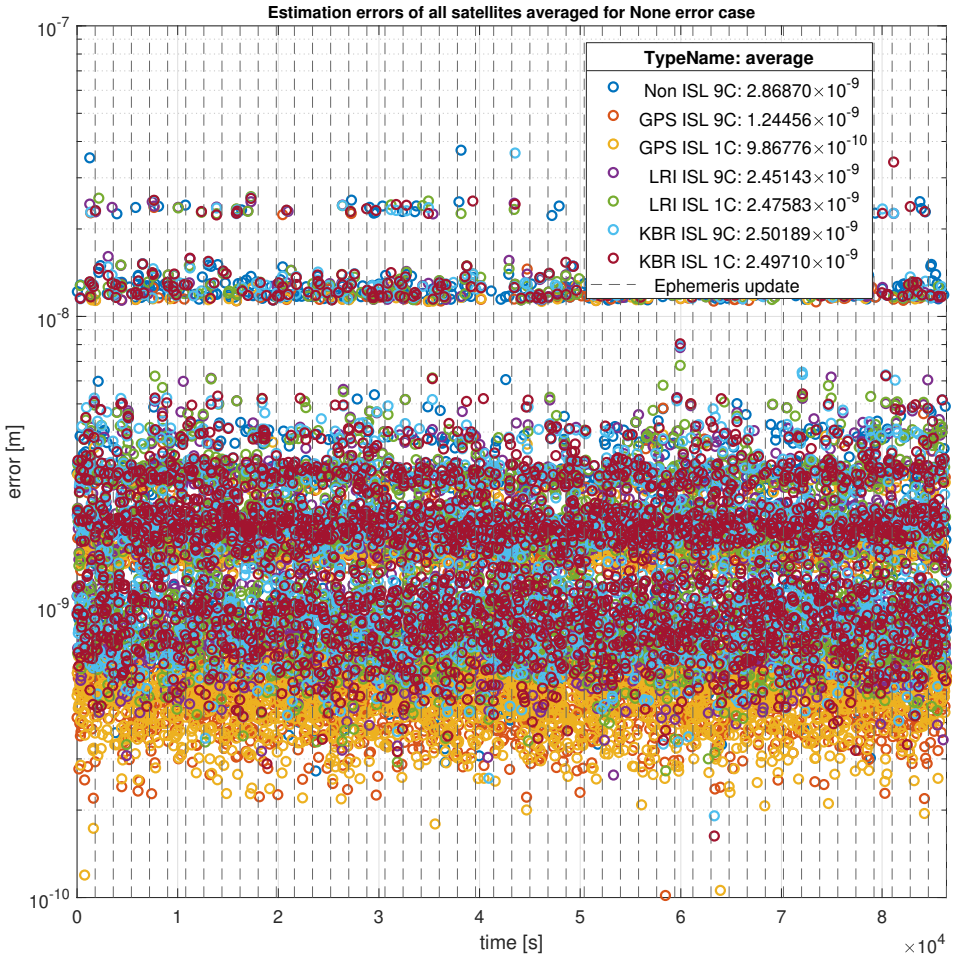

Figure A.1: Estimation errors of the estimation algorithms for an error-free simulation case

study follows this example below. Table A.1 and Table A.2 give the input data for this example problem. The first table gives the true state of the user to be estimated and the a priori guess. The second table gives the positions of the navigation satellites and the measured range from those satellites.

Navigation Satellites	X [m]	Y [m]	Z [m]	time [m]
True State	6,378,137.0	0.0	0.0	85,000.0
A Priori State	6,377,000.0	3,000.0	4,000.0	0.0

Table A.1: True state of the user and a priori position and clock estimate

Navigation Satellites	X [m]	Y [m]	Z [m]	Measured Range [m]
SV 01	22,808,160.9	-12,005,866.6	-6,609,526.5	21,480,623.2
SV 02	21,141,179.5	-2,355,056.3	-15,985,716.1	21,971,919.2
SV 08	20,438,959.3	-4,238,967.1	16,502,090.2	22,175,603.9
SV 14	18,432,296.2	-18,613,382.5	-4,672,400.8	22,747,561.5
SV 17	21,772,117.8	13,773,269.7	6,656,636.4	21,787,252.3
SV 23	15,561,523.9	3,469,098.6	-21,303,596.2	23,541,613.4
SV 24	13,773,316.6	15,929,331.4	-16,266,254.4	24,022,907.4

Table A.2: Positions and measured range of navigation satellites

With this data, first, the computed ranges to the navigation satellites are determined. These are shown in Table A.3. A small deviation from the book is seen in the computed range of the first navigation satellite. Presumably, this is caused by rounding of intermediate results in the book as the algorithm does not do this.

	Computed Range [m]	Book Computed Range [m]
SV 01	21,399,407.9	21,399,408.0
SV 02	21,890,921.6	21,890,921.6
SV 08	22,088,910.4	22,088,910.4
SV 14	22,666,464.0	22,666,464.0
SV 17	21,699,943.6	21,699,943.6
SV 23	23,460,242.4	23,460,242.4
SV 24	23,938,978.9	23,938,978.9

Table A.3: Computed range between user and navigation satellites according to the algorithm and [10]

After that, the design matrix is determined. The matrix found with the algorithm and the matrix given in the book are shown in Table A.4. Only the value in the upper left corner of the algorithm matrix is different from the corresponding value from the book. However, this is only a small difference and is caused by the difference in the computation of the range and the rounding used in the book.

Algorithm Design Matrix				**Book Design Matrix**			
-0.767833	0.561178	0.309052	1	-0.767832	0.561178	0.309052	1
-0.674443	0.107718	0.730427	1	-0.674443	0.107718	0.730427	1
-0.636607	0.192041	-0.746895	1	-0.636607	0.192041	-0.746895	1
-0.531856	0.821318	0.206314	1	-0.531856	0.821318	0.206314	1
-0.709454	-0.634576	-0.306574	1	-0.709454	-0.634576	-0.306574	1
-0.391493	-0.147744	0.908243	1	-0.391493	-0.147744	0.908243	1
-0.308965	-0.665289	0.679655	1	-0.308965	-0.665289	0.679655	1

Table A.4: Design matrices of the numerical example

With the design matrix, the least-squares estimation can be applied to provide the correction for the a priori state. The entire process is repeated one more time in the book resulting in two state correction vectors and two state estimates, given in Table A.5. In these values, small variances appear as well, expected to originate in the differences in rounding throughout the estimation in the book.

Parameter	**1st State Correction**		**1st State Estimate**		**2nd State Correction**		**2nd State Estimate**	
Source	**Algorithm**	**Book**	**Algorithm**	**Book**	**Algorithm**	**Book**	**Algorithm**	**Book**
X [m]	1,131.7	1,131.8	6,378,131.7	6,378,131.8	-0.3	-0.3	6,378,131.4	6,378,131.5
Y [m]	-2,996.8	-2,996.8	3.2	3.2	0.1	0.1	3.4	3.3
X [m]	-3,993.1	-3,993.1	6.9	6.9	0.2	0.2	7.0	7.1
Total [m]	84,996.3	84,996.4	84,996.3	84,996.4	-0.6	-0.6	84,995.7	84,995.8

Table A.5: State corrections and state estimates of one iteration

Table A.6 shows the DOP values that are determined and the resulting actual error determined with the point positioning method. The DOP values of the algorithm are identical to the values mentioned in the book. The actual error values show deviations, but these are assumed to be caused by rounding.

Parameter	**DOP Values**		**Actual Error**	
Source	**Algorithm**	**Book**	**Algorithm**	**Book**
X [m]	3.0	3.0	-5.6	-5.5
Y [m]	0.8	0.8	3.4	3.2
X [m]	0.8	0.8	7.0	7.1
Total [m]	3.7	3.7	-4.3	-4.2

Table A.6: DOP values and actual errors of numerical example

The differences in the intermediate and final results shown in the tables are minimal and explained by rounding differences. The variation from the book is in the order of magnitude of decimetres, which are negligible compared to the order of magnitude of the positions. Hence, this numerical example provides an additional validation of the SPP algorithm created in this thesis work.

A.3. Analytical Verification

It is possible to compare intermediate results with analytical results of the same steps to provide another form of verification for the used algorithms. This section performs this comparison for the KOD ISL

algorithm as this is the most prominent algorithm, and it contains all the principles the other algorithms also use.

Recall that the first step of the estimation process is the determination of the design matrix **H**. This matrix is formed by the partial derivatives of the observations with respect to the estimation parameters. In the matrix, every row corresponds to an observation and a column to an estimation parameter. For KOD ISL that means that there are 36 columns for the x-, y- and z-coordinates and clock offset of the nine LPS satellites and several columns for the bias parameters.

If LPS1 in the first epoch is considered, it receives observations from 31 satellites among which the satellites mentioned in Table A.7. The table gives the positions of those satellites and LPS1 in the first epoch. For the LPS satellites, these are the estimates from the single KOD algorithm as these are the positions used in the estimation. The satellites correspond to the first and second GNSS observation and the third ISL observation. For this reason, the bias indices are 1, 2 and 26.

Satellite	x [m]	y [m]	z [m]
LPS1	1.400×10^7	7.375×10^{-9}	-3.363×10^{-9}
Galileo02	2.395×10^7	9.729×10^6	1.442×10^7
Galileo10	2.395×10^7	-9.729×10^6	-1.442×10^7
LPS4	1.395×10^7	1.276×10^{-8}	1.220×10^6

Table A.7: LPS1 and two satellites it receives observations from in the first epoch

This means that the partial derivatives of the first and second observation are given by Equation A.1 and Equation A.2 and show how the partial derivatives appear for a GNSS observation. Equation A.3 shows the partial derivative for an ISL observation. Note that the partial derivatives with respect to both LPS satellites participating in the link are taken as it should.

$$\frac{\partial h^{G_2}_{r_1,0}}{\partial \mathbf{y}_0} = \left(-0.496, -0.485, -0.720, 1, \mathbf{0}^T_{r_2}, \cdots, \mathbf{0}^T_{r_9}, -1_1, 0_2, \cdots, 0_M\right) \tag{A.1}$$

$$\frac{\partial h^{G_{10}}_{r_1,0}}{\partial \mathbf{y}_0} = \left(-0.496, 0.485, 0.720, 1, \mathbf{0}^T_{r_2}, \cdots, \mathbf{0}^T_{r_9}, 0_1, -1_2, 0_3, \cdots, 0_M\right) \tag{A.2}$$

$$\frac{\partial h^{r_4}_{r_1,0}}{\partial \mathbf{y}_0} = \left(0.044, 0, -0.999, 1, \mathbf{0}^T_{r_2}, \mathbf{0}^T_{r_3}, -0.044, 0, 0.999, -1, \mathbf{0}^T_{r_5}, \cdots, \mathbf{0}^T_{r_9}, 0_1, \cdots, -1_{26}, \cdots, 0_M\right) \tag{A.3}$$

The values shown in the equations are indeed the values that the algorithm produces, thereby verifying the first step. Following this method provides a very characteristic structure of the design matrix considering that the partial derivatives form its rows. Figure A.2 shows the structure of the part of the design matrix corresponding to the first epoch and LPS1. The dotted line is the line between the satellites' state parameters and the bias parameters. The structure is exactly as one would expect and gives another means of verification of the written algorithm.

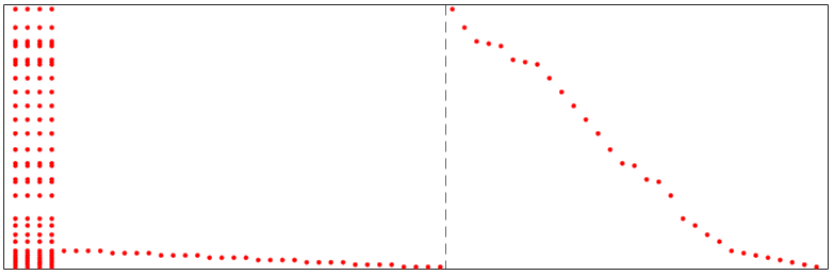

Figure A.2: The part of the design matrix corresponding to LPS1 in the first epoch visualised

The multiplication of the transpose of the design matrix, the weight matrix and the design matrix follows to obtain the normal matrix. Doing this for the nine LPS satellites provide the structures visualised in Figure A.3. In the figures, the dashed line denotes the distinction of the matrix parts corresponding

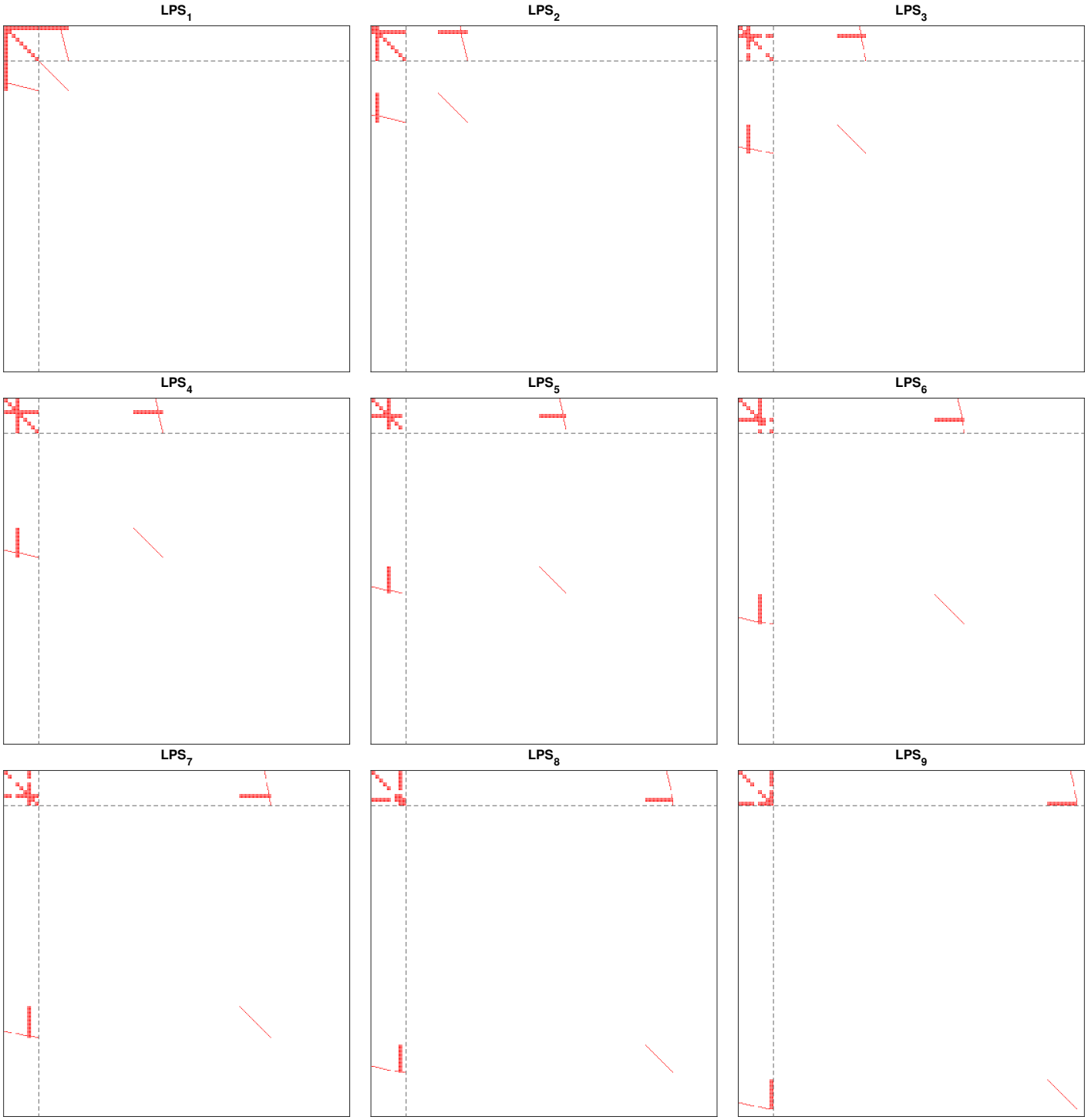

Figure A.3: The structures of the normal matrices of the first epoch of the nine LPS satellites

to the positions and clock offsets, the bias parameters or both. The former is placed in the left top and the second in the right bottom part.

Combining the matrices for the satellites grants the complete normal matrix, visualised in Figure A.4a. In the upper left corner a 36-by-36 block is visible corresponding to the positions and clock offsets of the satellites. Because only one epoch is visualised, only one 36-by-36 block is visible. The upper right part is the transpose of the lower left side of the matrix, and they correspond to the interconnection of the positions and clock offsets through the biases. The parts show very distinctive structures

for the ISL application in position estimation.

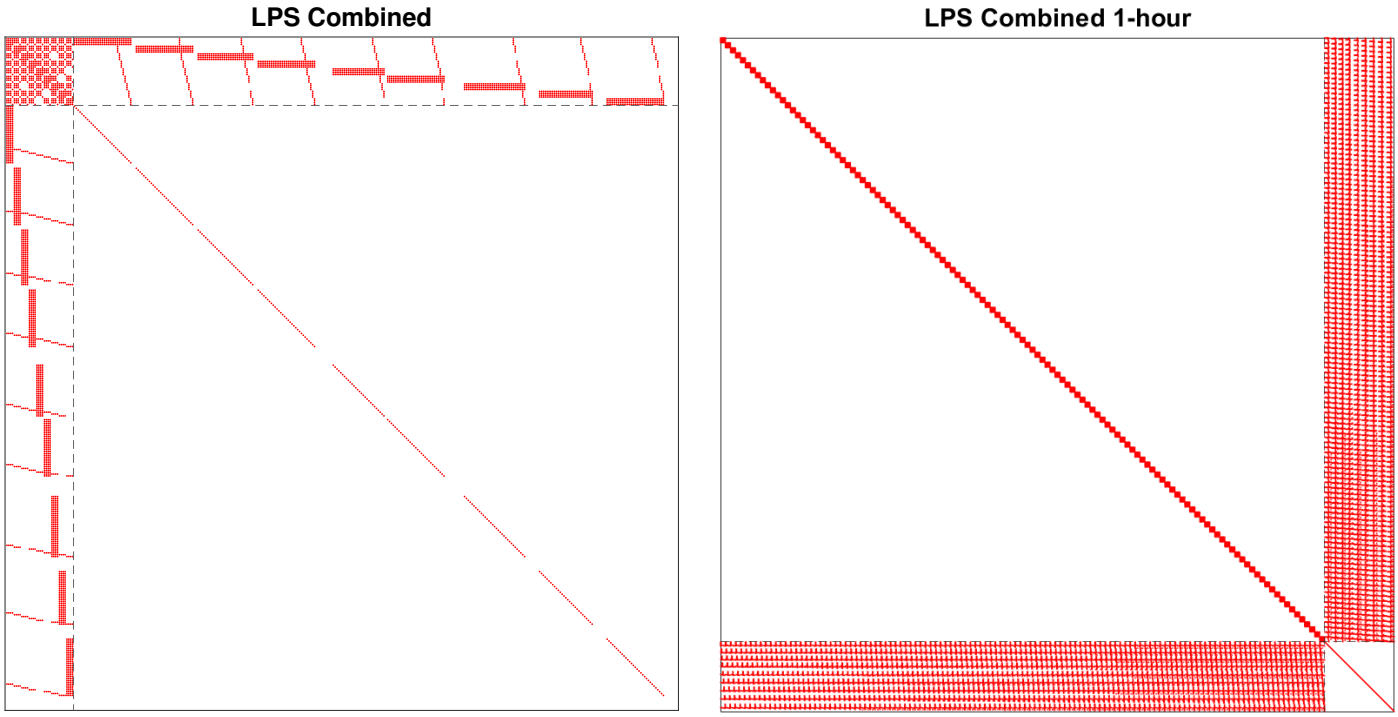

(a) Normal matrix of the nine satellites combined for the first epoch

(b) Normal matrix of the nine satellites combined for an 1-hour data arc

Figure A.4: The structures of the normal matrices of the first epoch and of a 1-hour data arc of the LPS satellites combined

If a data arc of one hour is taken to visualise the structure of the normal matrix of the KODISL algorithm, the structure in Figure A.4b is obtained. The upper left part of the matrix now consists of 121 36-by-36 sub-matrices on the diagonal. The structure obtained by the analytical approach matches perfectly with the structure obtained through the algorithm, as shown in the paper. Thereby, this approach contributes to the verification of the KODISL algorithm.

B

Orbital Parameters

This appendix provides the initial Kepler elements of all the satellites simulated in this thesis work.

	a [m]	e [-]	i [rad]	ω [rad]	Ω [rad]	θ [rad]
LPS1	1.400×10^7	0	0.000	0	0.000	0.000
LPS2	1.400×10^7	0	0.000	0	0.000	2.094
LPS3	1.400×10^7	0	0.000	0	0.000	4.189
LPS4	1.400×10^7	0	1.571	0	0.000	0.087
LPS5	1.400×10^7	0	1.571	0	6.283	2.182
LPS6	1.400×10^7	0	1.571	0	6.283	4.276
LPS7	1.400×10^7	0	1.571	0	1.571	0.000
LPS8	1.400×10^7	0	1.571	0	1.571	2.094
LPS9	1.400×10^7	0	1.571	0	1.571	4.189

Table B.1: Initial Kepler elements of the LPS constellation

	a [m]	e [-]	i [rad]	ω [rad]	Ω [rad]	θ [rad]
BeiDou01	2.788×10^7	0	0.974	0	0.000	0.000
BeiDou02	2.788×10^7	0	0.974	0	0.000	0.698
BeiDou03	2.788×10^7	0	0.974	0	0.000	1.396
BeiDou04	2.788×10^7	0	0.974	0	6.283	2.094
BeiDou05	2.788×10^7	0	0.974	0	0.000	2.793
BeiDou06	2.788×10^7	0	0.974	0	0.000	3.491
BeiDou07	2.788×10^7	0	0.974	0	0.000	4.189
BeiDou08	2.788×10^7	0	0.974	0	0.000	4.887
BeiDou09	2.788×10^7	0	0.974	0	0.000	5.585
BeiDou10	2.788×10^7	0	0.974	0	2.094	0.000
BeiDou11	2.788×10^7	0	0.974	0	2.094	0.698
BeiDou12	2.788×10^7	0	0.974	0	2.094	1.396
BeiDou13	2.788×10^7	0	0.974	0	2.094	2.094
BeiDou14	2.788×10^7	0	0.974	0	2.094	2.793
BeiDou15	2.788×10^7	0	0.974	0	2.094	3.491
BeiDou16	2.788×10^7	0	0.974	0	2.094	4.189
BeiDou17	2.788×10^7	0	0.974	0	2.094	4.887
BeiDou18	2.788×10^7	0	0.974	0	2.094	5.585
BeiDou19	2.788×10^7	0	0.974	0	4.189	0.000
BeiDou20	2.788×10^7	0	0.974	0	4.189	0.698
BeiDou21	2.788×10^7	0	0.974	0	4.189	1.396
BeiDou22	2.788×10^7	0	0.974	0	4.189	2.094
BeiDou23	2.788×10^7	0	0.974	0	4.189	2.793
BeiDou24	2.788×10^7	0	0.974	0	4.189	3.491
BeiDou25	2.788×10^7	0	0.974	0	4.189	4.189
BeiDou26	2.788×10^7	0	0.974	0	4.189	4.887
BeiDou27	2.788×10^7	0	0.974	0	4.189	5.585

Table B.2: Initial Kepler elements of the BeiDou constellation

	a [m]	e [-]	i [rad]	ω [rad]	Ω [rad]	θ [rad]
Galileo01	2.960×10^7	0	0.977	0	0.000	0.000
Galileo02	2.960×10^7	0	0.977	0	0.000	0.628
Galileo03	2.960×10^7	0	0.977	0	6.283	1.257
Galileo04	2.960×10^7	0	0.977	0	0.000	1.885
Galileo05	2.960×10^7	0	0.977	0	0.000	2.513
Galileo06	2.960×10^7	0	0.977	0	0.000	3.142
Galileo07	2.960×10^7	0	0.977	0	0.000	3.770
Galileo08	2.960×10^7	0	0.977	0	0.000	4.398
Galileo09	2.960×10^7	0	0.977	0	0.000	5.027
Galileo10	2.960×10^7	0	0.977	0	0.000	5.655
Galileo11	2.960×10^7	0	0.977	0	2.094	0.000
Galileo12	2.960×10^7	0	0.977	0	2.094	0.628
Galileo13	2.960×10^7	0	0.977	0	2.094	1.257
Galileo14	2.960×10^7	0	0.977	0	2.094	1.885
Galileo15	2.960×10^7	0	0.977	0	2.094	2.513
Galileo16	2.960×10^7	0	0.977	0	2.094	3.142
Galileo17	2.960×10^7	0	0.977	0	2.094	3.770
Galileo18	2.960×10^7	0	0.977	0	2.094	4.398
Galileo19	2.960×10^7	0	0.977	0	2.094	5.027
Galileo20	2.960×10^7	0	0.977	0	2.094	5.655
Galileo21	2.960×10^7	0	0.977	0	4.189	0.000
Galileo22	2.960×10^7	0	0.977	0	4.189	0.628
Galileo23	2.960×10^7	0	0.977	0	4.189	1.257
Galileo24	2.960×10^7	0	0.977	0	4.189	1.885
Galileo25	2.960×10^7	0	0.977	0	4.189	2.513
Galileo26	2.960×10^7	0	0.977	0	4.189	3.142
Galileo27	2.960×10^7	0	0.977	0	4.189	3.770
Galileo28	2.960×10^7	0	0.977	0	4.189	4.398
Galileo29	2.960×10^7	0	0.977	0	4.189	5.027
Galileo30	2.960×10^7	0	0.977	0	4.189	5.655

Table B.3: Initial Kepler elements of the Galileo constellation

	a [m]	e [-]	i [rad]	ω [rad]	Ω [rad]	θ [rad]
GLONASS01	2.548×10^7	0	1.131	0	0.000	0.000
GLONASS02	2.548×10^7	0	1.131	0	0.000	0.785
GLONASS03	2.548×10^7	0	1.131	0	6.283	1.571
GLONASS04	2.548×10^7	0	1.131	0	6.283	2.356
GLONASS05	2.548×10^7	0	1.131	0	0.000	3.142
GLONASS06	2.548×10^7	0	1.131	0	0.000	3.927
GLONASS07	2.548×10^7	0	1.131	0	6.283	4.712
GLONASS08	2.548×10^7	0	1.131	0	6.283	5.498
GLONASS09	2.548×10^7	0	1.131	0	2.094	6.283
GLONASS10	2.548×10^7	0	1.131	0	2.094	0.785
GLONASS11	2.548×10^7	0	1.131	0	2.094	1.571
GLONASS12	2.548×10^7	0	1.131	0	2.094	2.356
GLONASS13	2.548×10^7	0	1.131	0	2.094	3.142
GLONASS14	2.548×10^7	0	1.131	0	2.094	3.927
GLONASS15	2.548×10^7	0	1.131	0	2.094	4.712
GLONASS16	2.548×10^7	0	1.131	0	2.094	5.498
GLONASS17	2.548×10^7	0	1.131	0	4.189	0.000
GLONASS18	2.548×10^7	0	1.131	0	4.189	0.785
GLONASS19	2.548×10^7	0	1.131	0	4.189	1.571
GLONASS20	2.548×10^7	0	1.131	0	4.189	2.356
GLONASS21	2.548×10^7	0	1.131	0	4.189	3.142
GLONASS22	2.548×10^7	0	1.131	0	4.189	3.927
GLONASS23	2.548×10^7	0	1.131	0	4.189	4.712
GLONASS24	2.548×10^7	0	1.131	0	4.189	5.498

Table B.4: Initial Kepler elements of the GLONASS constellation

	a [m]	e [-]	i [rad]	ω [rad]	Ω [rad]	θ [rad]
GPS01	2.658×10^7	0	0.960	0	0.000	0.000
GPS02	2.658×10^7	0	0.960	0	0.000	0.524
GPS03	2.658×10^7	0	0.960	0	6.283	2.356
GPS04	2.658×10^7	0	0.960	0	6.283	4.451
GPS05	2.658×10^7	0	0.960	0	1.047	0.000
GPS06	2.658×10^7	0	0.960	0	1.047	0.524
GPS07	2.658×10^7	0	0.960	0	1.047	2.356
GPS08	2.658×10^7	0	0.960	0	1.047	4.451
GPS09	2.658×10^7	0	0.960	0	2.094	0.000
GPS10	2.658×10^7	0	0.960	0	2.094	0.524
GPS11	2.658×10^7	0	0.960	0	2.094	2.356
GPS12	2.658×10^7	0	0.960	0	2.094	4.451
GPS13	2.658×10^7	0	0.960	0	3.142	6.283
GPS14	2.658×10^7	0	0.960	0	3.142	0.524
GPS15	2.658×10^7	0	0.960	0	3.142	2.356
GPS16	2.658×10^7	0	0.960	0	3.142	4.451
GPS17	2.658×10^7	0	0.960	0	4.189	0.000
GPS18	2.658×10^7	0	0.960	0	4.189	0.524
GPS19	2.658×10^7	0	0.960	0	4.189	2.356
GPS20	2.658×10^7	0	0.960	0	4.189	4.451
GPS21	2.658×10^7	0	0.960	0	5.236	0.000
GPS22	2.658×10^7	0	0.960	0	5.236	0.524
GPS23	2.658×10^7	0	0.960	0	5.236	2.356
GPS24	2.658×10^7	0	0.960	0	5.236	4.451

Table B.5: Initial Kepler elements of the GPS constellation

C

Software Dependencies

This appendix states the software used in the thesis work and links to the GitHub page where the source code can be found of the tools built for the research.

For this thesis work, the following software has been used.

- QtCreator 4.11.0[1]
- CMake 3.15.3[2]
- MATLAB R2019b[3]
- Tudat[4] [5] (updated in September 2019)

The source code for the simulation and estimation tool written for this thesis work is found at:

`https://github.com/Casperbru/pecmeoLPS`

[1] `https://www.qt.io/`
[2] `https://cmake.org/`
[3] `https://nl.mathworks.com/`
[4] `http://tudat.tudelft.nl/`
[5] `https://github.com/Tudat/tudat`

Bibliography

[1] Jack O Burns, Benjamin Mellinkoff, Matthew Spydell, Terrence Fong, David A Kring, William D Pratt, Timothy Cichan, and Christine M Edwards. Science on the lunar surface facilitated by low latency telerobotics from a lunar orbital platform-gateway. *Acta Astronautica*, 154:195–203, 2019.

[2] Seisuke Fukuda, Shin-ichiro Sakai, Eiichi Sato, Shujiro Sawai, and SLIM WG. SLIM: Small explorer for technology demonstration of lunar pinpoint landing. In *The 24th Workshop on JAXA Astrodynamics and Flight Mechanics*, page 109, 2014.

[3] Tracy Gill. Nasa's lunar orbital platform-gateway. In *The Space Congress Proceedings 2018 (45th): The Next Great Steps*, pages 4–17, February 2018.

[4] Jitendra Nath Goswami and Mylswamy Annadurai. Chandrayaan-2 mission. In *Lunar and Planetary Science Conference*, volume 42, page 2042, 2011.

[5] M A Griffioen. Assessment of Lunar Positioning Accuracy with PECMEO Navigation Satellites. type, TU Delft, Kluyverweg 1, Delft, 2020. note.

[6] Elliott Kaplan and Christopher Hegarty. *Understanding GPS: principles and applications*. Artech house, 2nd edition, 2006.

[7] Kroes, R. *Precise Relative Positioning of Formation Flying Spacecraft using GPS*. PhD thesis, Delft University of Technology, April 2006. URL `http://resolver.tudelft.nl/uuid:1a68ee94-3d55-44b9-9d8b-25fa44e96922`.

[8] Thomas M Perrin and James G Casler. Architecture study for a fuel depot supplied from lunar resources. In *AIAA SPACE 2016*, page 5306. Aerospace Research Central, 2016.

[9] Dong-Young Rew, Gwanghyeok Ju, Sangchul Lee, Kwangjin Kim, Sang-Wook Kang, and Sang-Ryool Lee. Control system design of the korean lunar lander demonstrator. *Acta Astronautica*, 94 (1):328–337, 2014.

[10] James J Spilker Jr, Penina Axelrad, Bradford W Parkinson, and Per Enge. *Global Positioning System: Theory and Applications, Volume I*. American Institute of Aeronautics and Astronautics, 1996.

[11] Fabio Tronchetti. The moon agreement in the 21st century: Addressing its potential role in the era of commercial exploitation of the natural resources of the moon and other celestial bodies. *J. Space L.*, 36:489, 2010.

[12] Qiong Wang and Jizhong Liu. A chang'e-4 mission concept and vision of future chinese lunar exploration activities. *Acta astronautica*, 127:678–683, 2016.